

## Original Article

**Cite this article:** Hryniewicz K, Miyajima Y, Amano K, Georgieva MN, Jakubowicz M, Jenkins RG, and Kaim A (2021) Formation, diagenesis and fauna of cold seep carbonates from the Miocene Taishu Group of Tsushima (Japan). *Geological Magazine* **158**: 964–984. <https://doi.org/10.1017/S001675682000103X>


Received: 29 March 2020  
Revised: 11 August 2020  
Accepted: 24 August 2020  
First published online: 14 October 2020

**Keywords:**

bathymodiolin mussels; hydrocarbons; methane-derived authigenic carbonates; Sea of Japan; seep fauna; stable isotopes; vesicomid bivalves

**Author for correspondence:** Krzysztof Hryniewicz, Email: [krzyszth@twarda.pan.pl](mailto:krzyszth@twarda.pan.pl)

# Formation, diagenesis and fauna of cold seep carbonates from the Miocene Taishu Group of Tsushima (Japan)

Krzysztof Hryniewicz<sup>1</sup> , Yusuke Miyajima<sup>2</sup>, Kazutaka Amano<sup>3</sup>, Magdalena N Georgieva<sup>4</sup>, Michał Jakubowicz<sup>5</sup>, Robert G Jenkins<sup>6</sup> and Andrzej Kaim<sup>1</sup>

<sup>1</sup>Institute of Paleobiology, Polish Academy of Sciences, ul. Twarda 51/55, PL-00-818 Warsaw, Poland; <sup>2</sup>Geological Survey of Japan, National Institute of Advanced Industrial Science and Technology (AIST), Central 7, 1-1-1 Higashi, Tsukuba, Ibaraki 305-8567, Japan; <sup>3</sup>Department of Geoscience, Joetsu University of Education, 1 Yamayashiki, 943-8512, Joetsu, Japan; <sup>4</sup>Department of Life Sciences, Natural History Museum, London, UK; <sup>5</sup>Isotope Research Unit, Adam Mickiewicz University, ul. B. Krygowskiego 10, PL-61-680 Poznań, Poland and <sup>6</sup>College of Science and Engineering, Kanazawa University, Kakuma, Kanazawa, Ishikawa 920-1192, Japan

**Abstract**

The studied seep carbonates from Tsushima, Japan, are embedded within marine siliciclastics of the lower Miocene Taishu Group and represent the earliest evidence of hydrocarbon seepage in the Sea of Japan. In contrast to Miocene and Pliocene examples from Honshu, which are often found above anticlines, the seeps from Tsushima formed within a pull-apart basin before major anticlines had formed. The three carbonates from Fukuzaki, Kanoura and Tanohama are composed chiefly of calcite, with significant admixture of ankerite only at Kanoura. The stable carbon isotope composition of calcites ( $\delta^{13}\text{C}$  as low as  $-40.2\text{‰}$  VPDB for Fukuzaki,  $-41.8\text{‰}$  VPDB for Kanoura, and  $-52.8\text{‰}$  VPDB for Tanohama) indicate methanogenic origin of the carbonates. Textures of these deposits, including radial and yellow cements, are indicative of formation at a methane seep. The stable oxygen isotope composition of calcites ( $\delta^{18}\text{O}$  values as low as  $-14.4\text{‰}$  VPDB for Fukuzaki,  $-14.5\text{‰}$  VPDB for Kanoura and  $-13.9\text{‰}$  VPDB for Tanohama) indicate that they were influenced by burial fluids. Burial diagenesis is also indicated by the stable isotopic compositions of ankerite ( $\delta^{13}\text{C}$  ranging from  $-19.1\text{‰}$  to  $-7.1\text{‰}$  VPDB,  $\delta^{18}\text{O}$  from  $-11.1\text{‰}$  to  $-9.7\text{‰}$  VPDB). Molecular fossils from Tanohama comprise *n*-alkanes with short-chain predominance, interpreted to have formed due to thermal cracking of organic matter. The carbonates yield a chemosynthesis-based community comprising vesicomids *Pleurophopsis chitanii*, *P. cf. hamuroi*, the bathymodiolin '*Bathymodiolus*' *akanudaensis*, the lucinid *Lucinoma* sp. and the provannid *Provanna?* sp., which have never been hitherto identified. '*Bathymodiolus*' *akanudaensis*, *Lucinoma* sp. and *Provanna?* sp. are the oldest records of these taxa in the Sea of Japan.

**1. Introduction**

In marine environments, subsurface hydrocarbon generation, migration and release lead to formation of submarine cold seeps—sites where hydrocarbon-charged fluids are released into the water column (Campbell, 2006). Reduced compounds available at such sites are a resource for a lush macrofauna, chiefly chemosymbiotic bivalves and polychaete tubeworms (Dubilier *et al.* 2008), and diverse asymbiotic species supported by organic matter produced due to chemosynthesis. Apart from the fauna, another distinct feature of submarine hydrocarbon emissions is precipitations of authigenic carbonates, which form due to the process of microbially mediated anaerobic oxidation of methane (AOM; Boetius *et al.* 2000). Due to their peculiar formation mechanisms, the methane-derived authigenic carbonates are typified by distinct geochemical and petrographic features, such as depletion in  $^{13}\text{C}$ , presence of  $^{13}\text{C}$ -depleted biomarkers typical of AOM-mediating microbial consortia, as well as lithological textures indicative of microbially facilitated carbonate formation (Peckmann & Thiel, 2004). Thanks to the above, carbonates formed at ancient seep sites can be rather easily recognized in the fossil record long after hydrocarbon seepage ceased (e.g. Peckmann *et al.* 1999, 2003, 2009, 2011; Himmler *et al.* 2008; Amano *et al.* 2010; Hammer *et al.* 2011; Hryniewicz *et al.* 2015, 2016; Kiel & Hansen, 2015; Miyajima *et al.* 2016, 2018; Jakubowicz *et al.* 2017; cf. Campbell, 2006).

Numerous fossil hydrocarbon seep carbonates and associated faunas have been previously reported from Japan (e.g. Hikida *et al.* 2003; Jenkins *et al.* 2007; Amano *et al.* 2010, 2013; Miyajima *et al.* 2016, 2017, 2018; cf. Majima *et al.* 2005). They span from late Early Cretaceous (Albian; Kaim *et al.* 2009) to Pleistocene in age, with nearly 100 sites listed in the last comprehensive review by Majima *et al.* (2005). A long-lasting record of ancient hydrocarbon seepage along the

eastern (presently Pacific) shores of Japan in part reflects its geological history, where the active continental margin was especially predisposed for seabed fluid release (Sibuet & Olu, 1998). The western (Sea of Japan) side of the Japanese Islands, on the other hand, was formed by complex tectonics during the Miocene, or perhaps earlier (Lallemand & Jolivet, 1985; Ingle, 1992; Nakada *et al.* 1997), with development of the back-arc basin and its subsequent inversion. This process is traceable there by a seepage history, with ancient seep deposits as old as the middle Miocene recording release of hydrocarbons to marine environments (Majima *et al.* 2005; Amano *et al.* 2013; Miyajima *et al.* 2017). Extant hydrocarbon seeps in the Sea of Japan offshore Niigata Prefecture, central Honshu, where hydrocarbon gases are released from breached anticlines along fault planes (Okui *et al.* 2008), can be regarded as structural equivalents of some Miocene and Pliocene seeps, which have likely formed in similar structural settings (e.g. Amano & Kanno, 2005; Amano *et al.* 2010; Amano & Jenkins, 2011a; Miyajima *et al.* 2018). Until now, the oldest chemosynthetic fauna in the Sea of Japan is from the lower Miocene Kurosedani Formation in Toyama Prefecture, central Honshu (Amano *et al.* 2019b). However, it is not associated with any carbonates indicating hydrocarbon seepage. In order to understand the relation between seepage activity and the formation of the Sea of Japan, it is necessary to examine any lower Miocene seep carbonates with chemosynthetic faunas from the Sea of Japan side.

In this paper we present a description of three seep carbonates from the lower Miocene Taishu Group, cropping out on the Tsushima islands, located at the western entrance of the Sea of Japan (Fig. 1). The Tsushima islands are located between the Eurasian continent and Japanese Islands, and are therefore important in understanding the ancient seep systems during the opening of the Sea of Japan back-arc basin. The carbonate bodies and associated chemosynthesis-based faunas from the Taishu Group have been previously reported by Ninomiya (2011, 2012) and Ninomiya *et al.* (2020) at four sites, along with the isotopic evidence for seep-related identity of two of these deposits (Ninomiya, 2012;

Ninomiya *et al.* 2020). However, these tentative identifications of the chemosynthetic species are based on ill-preserved shells, which, in our opinion, allow for identification to the generic level only. Our study includes identification of chemosynthetic species to the species level based on better-preserved materials, and presents a comprehensive description of petrography, stable isotope geochemistry and organic geochemistry of three of the four known carbonate deposits from Tsushima. We also use optical and cathodoluminescence (CL) microscope imagery to reveal the degree of diagenetic alteration in these seep carbonates, and discuss the results in the general context of the diagenetic history of the Taishu Group. Finally, we place the seep carbonates of the Taishu Group in a broader geological context. As the lower Miocene seep carbonates from the Taishu Group are the oldest seep deposits from the Sea of Japan, we discuss early Miocene hydrocarbon seepage in Tsushima in relation to the geological events that shaped the Sea of Japan into the form seen today.

## 2. Geological setting

Tsushima is located within the Korean Strait separating the island of Kyushu from the Korean Peninsula (Fig. 1). The two major islands forming Tsushima are Shimojima and Kamishima, and both are almost entirely composed of folded siliciclastics of the Taishu Group (Fig. 1) with subordinate volcanic tuffs, porphyric intrusives and rhyolite lavas (Miti, 1972, 1973, 1974). The group comprises three lithostratigraphic units, customarily called the Lower, Middle and Upper formations (Fig. 2), representing a succession of mudstones, sandstones and conglomerates deposited under marine and estuarine conditions influenced by northward-prograding river deltas (e.g. Nakajo, 1998; Nakajo & Maejima, 1998; Ninomiya *et al.* 2014, 2020). The bulk of the Taishu Group represents marine sediments accumulated due to landslide activity in the palaeo-Tsushima Basin formed by pull-apart tectonics in the SW Sea of Japan. The materials supplied

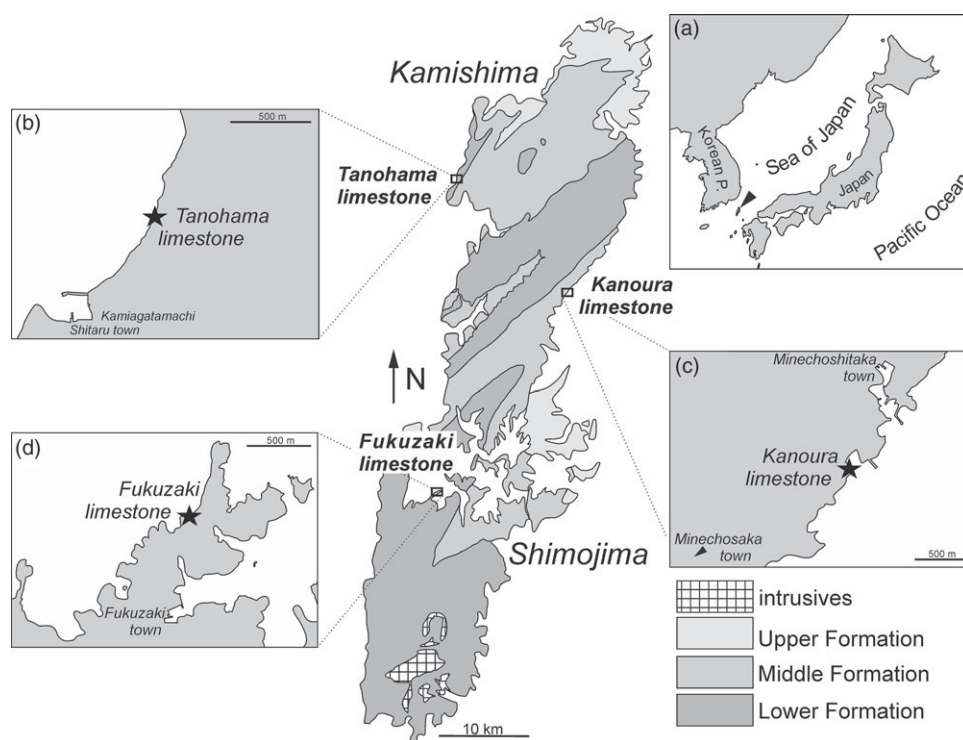


**Fig. 1.** Study area and geological map of Tsushima, simplified after Miti (1972, 1973, 1974) and Ninomiya *et al.* (2014). (a) Inset map with location of study area indicated. (b–d) Map showing location of Tanohama (b), Kanoura (c) and Fukuzaki (d) limestones.

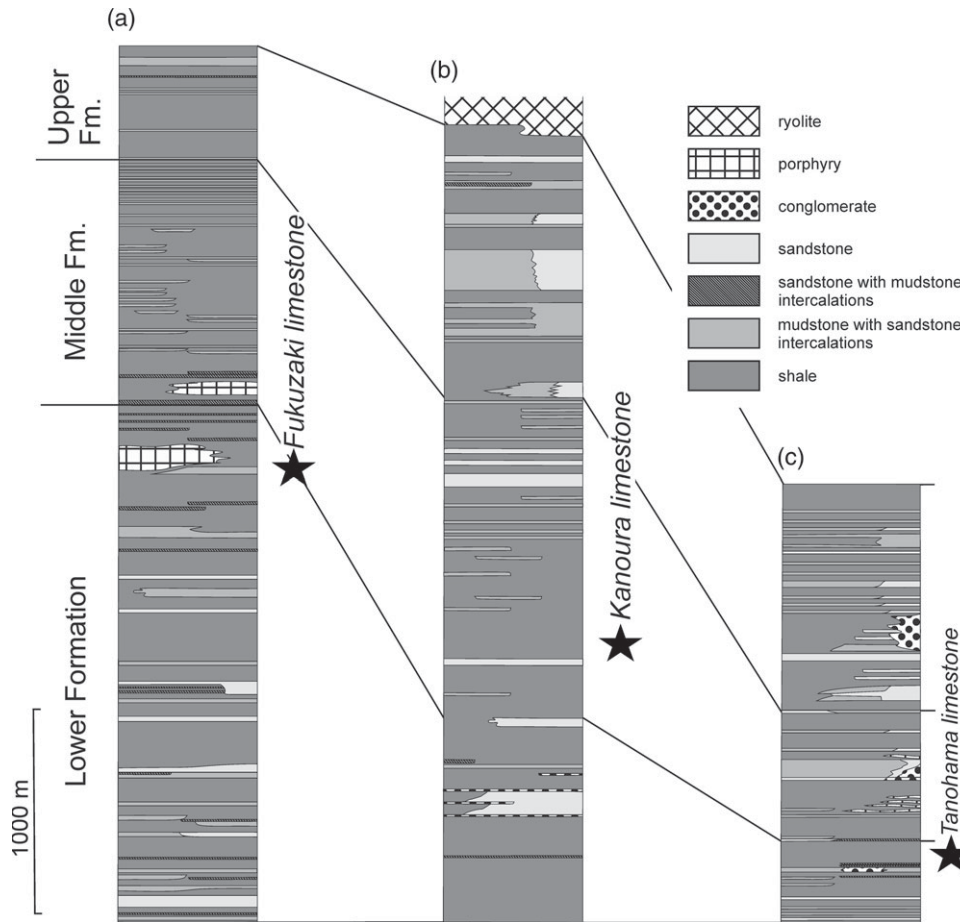


**Fig. 2.** Uncorrelated lithological columns of the Taishu Group in the southern (a), central (b) and northern (c) parts of Tsushima, with approximate stratigraphic position of the studied seep deposits indicated. Lithological columns after Miti (1972, 1973, 1974), stratigraphic position of the seep deposits after Ninomiya (2011).

by submarine landslides came from surrounding shallow shelf areas and were transported to the base of the continental slope at a high sedimentation rate (Golozubov *et al.* 2017). The palaeobathymetric estimates for at least the lower parts of the Taishu Group indicate water depths exceeding 800 m (Ninomiya *et al.* 2020).

Before the description of chemosymbiotic bivalves by Ninomiya (2011), many normal shallow- and deep-water molluscan fossils from the Taishu Group had been recorded by Kanno (1955) and Masuda (1970). According to Masuda (1970), the shallow-water faunas including *Mizuhopecten cf. kimurai murayamai* (Yokoyama) occurred in the lower part, and the deep-water faunas including protobranchs and mud pectens in the middle and upper parts of the Taishu Group. The chemosynthetic bivalves from the Fukuzaki (mistakenly referred to as Fukusaki), Tanohama and Kanoura Limestones have been described in ascending order by Ninomiya (2011, 2012) and Ninomiya *et al.* (2020). The former two limestones occur in the uppermost part of the Lower Formation while the Kanoura Limestone has a position near the lowermost part of the Middle Formation (Fig. 2).

Dating of the Taishu Group has been a matter of controversy for some time (cf. Sakai & Nishi, 1990). Poorly preserved Palaeogene microfossils found in the Lower and Upper formations of the group (e.g. Nakajo & Funakawa, 1996), considered as an evidence of its Palaeogene age (e.g. Sakai & Nishi, 1990), were likely redeposited from older rocks. Palynological materials examined are diagenetically altered and did not provide any identifiable fossils (E Durska, pers. comm. 2019), thus excluding palynology as a

dating tool for the Taishu Group. The Ebashima Formation unconformably overlying the Group yields Pliocene foraminifers (Isomi & Nagahama, 1964), confining the upper age limit of the Taishu Group to pre-Pliocene. U–Pb radiometric dating of the Kunehama Tuff from the lowermost part of the Taishu Group yielded an absolute age of 17.9 Ma, whereas the Oobaura Tuff from the uppermost part of the unit has an age of 15.9 Ma (Ninomiya *et al.* 2014). An early Miocene age for at least fragments of the Taishu Group can therefore be postulated. Nevertheless, mutual stratigraphic relationships between the Lower, Middle and Upper formations cropping out in various parts of the islands remain to be established, and the age relationships between the three seep deposits discussed in this paper are unknown.

### 3. Materials and methods

We collected carbonate and fossil samples from three sites, Fukuzaki, Kanoura and Tanohama (Fig. 1). Another limestone body has been previously reported by Ninomiya (2011, 2012) at Nita, but we could not find this limestone during our field survey in 2016.

A set of uncovered thin-sections (48 mm × 28 mm) and polished slabs were prepared in order to identify the main carbonate phases, and to interpret spatial and temporal relationships between them. Thin-sections were analysed under normal and cross-polarized light using an optical microscope. Some polished and carbon-coated thin-sections were examined with a CL microscope equipped with a hot cathode linked to the Kappa video camera for recording digital images at the Institute of Paleobiology of

the Polish Academy of Sciences in Warsaw. An electron energy of 14 keV and a beam current of 0.1–0.2 mA were used.

Invertebrate fossils were prepared with a vibrotol and coated with ammonium chloride before photography. Measurements were taken with a digital caliper with precision of 0.1 mm.

The mineralogical composition of the investigated seep carbonates was determined using X-ray powder diffractometry (XRD) with the Thermo Electron ALR X'tra powder diffractometer at the Institute of Geology of the Adam Mickiewicz University, Poznań (Poland). The instrument operated at a tube voltage of 40 kV and a tube current of 30 mA. The spectrum was obtained for an angular range of 3–65° 2 $\theta$  with a 0.02° 2 $\theta$  step.

Powdered samples for carbon and oxygen isotope analyses were collected from slabs using a hand-held microdrill and analysed by a Thermo Scientific GasBench II/Delta V Advantage isotope ratio mass spectrometer (IRMS) at the Laboratory of Evolution of Earth Environment, Kanazawa University (LEEKU), Kanazawa, Japan, or a Thermo Scientific GasBench II/Delta Plus IRMS at the Department of Earth and Planetary Science, the University of Tokyo, Tokyo, Japan (EPSUT). The powders (~300–500  $\mu$ g) were reacted with orthophosphoric acid in a glass vial under helium atmosphere at 70 °C (LEEKU) or 60 °C (EPSUT) in an online GasBench II system. Samples containing ankerite were reacted for 72 hours at 60 °C. The produced CO<sub>2</sub> was analysed in a continuous-flow IRMS. All isotope values are reported in the  $\delta$  notation as a per-mil difference between the sample and a Vienna Pee Dee Belemnite (VPDB) standard in delta notation ( $[\delta = R_{\text{sample}}/R_{\text{standard}} - 1] \times 1000$ , where  $R$  is the ratio of minor to major isotopes). The measured values were calibrated with the international standard NBS19. At the LEEKU, the standard deviation of replicate analyses of NBS19 ( $n = 6$ ) and working standards LSVEC ( $n = 6$ ) and JLS-1 ( $n = 9$ ) during three analytical sessions was better than 0.11 ‰ and 0.09 ‰ for  $\delta^{13}\text{C}$  and  $\delta^{18}\text{O}$ , respectively. The standard deviation of ten replicate analyses of a working standard HRS-carb at the EPSUT was 0.16 ‰ and 0.23 ‰ for  $\delta^{13}\text{C}$  and  $\delta^{18}\text{O}$ , respectively.

Lipid biomarker analyses were performed following Miyajima *et al.* (2016) with modified extraction methods. After removal of weathered surfaces, small pieces of rock were washed in distilled water and then in methanol (MeOH) and dichloromethane (DCM) using an ultrasonic bath for 10 min. The washed pieces were crushed into fine chips, and then powdered using a tungsten mortar and pestle. Lipids were extracted from the powdered samples (~10 g powders) using a Thermo Scientific Accelerated Solvent Extractor System (Dionex ASE 350) at the LEEKU, with DCM as a solvent. For another ~10 g powder of a sample from Tanohama, hexane-washed distilled water was added to the powder and 1 N HCl was slowly poured to dissolve the carbonate. After the carbonate was dissolved, lipids were extracted by adding hexane: DCM (9:1, v:v) and centrifuging for 10 min (three cycles). The separated solvents were washed with hexane-washed distilled water. After removing elemental sulphur, the aliphatic hydrocarbon fractions of the extracted lipids were obtained through a silica gel column with *n*-hexane. Finally, the aliphatic hydrocarbon fractions were diluted with 200  $\mu$ L of *n*-hexane after drying. Individual compounds were detected using a gas chromatograph – mass spectrometer (Shimadzu GCMS-QP2010) equipped with a HP-5MS capillary column (30 m  $\times$  0.25 mm  $\times$  0.25  $\mu$ m; Agilent Technologies) at the LEEKU. The column oven temperature was increased from 50 °C to 120 °C at 30 °C/min, then from 120 °C to 310 °C at 3.0 °C/min, and kept at 310 °C for 15 min. The splitless system inlet was kept at 310 °C.

The stable carbon isotopic compositions of total organic carbon (TOC) within the seep carbonates were analysed for the powdered samples obtained at the same time as those for biomarker analyses. The carbonate powders (~1 g) were completely dissolved by reacting with 5 N HCl for 24 h at room temperature. Acid was then removed by repeated decantation after centrifugation and washing with deionized water. After freeze-drying, the residues (~4 mg) were analysed with a Thermo Quest NA2500NCS elemental analyser (EA) connected to a Thermo Scientific Delta V Advantage IRMS at the LEEKU. Samples were oxygenated at 1000 °C to make CO<sub>2</sub> gas. Concentrations of TOC (in wt %) were calculated by comparing measured <sup>44</sup>CO<sub>2</sub> peak areas with those of a working standard (L-alanine, LAL) containing 10  $\mu$ gC/ $\mu$ L. Carbon isotopic compositions are given in the  $\delta$  notation ( $\delta^{13}\text{C}$  ‰ vs VPDB). The standard deviation of 15 replicate analyses of LAL was 0.06 ‰.

### 3. Results

#### 4a. Fukuzaki limestone

##### 4.a.1. Locality description

The Fukuzaki seep deposit was found on the NW shore of a small peninsula, at the base of a cliff c. 700 m north of Fukuzaki Town on Shimojima at 34° 18' 21.24" N, 129° 15' 11.58" E (Fig. 1). In 2016 the deposit included an *in situ* carbonate body c. 5.6 m long and c. 0.3 m thick found in the cliff (see also Ninomiya *et al.* 2020) and numerous rounded boulders found on the beach (Fig. 3a). The deposit consists of indurated black limestone. We did not find any fossil in the carbonate body found *in situ*, whereas the boulders found on the beach contained worm tubes and bivalve fossils. All of the fossils and most of the rock samples studied herein came from the boulders.

##### 4.a.2. Mineralogy, stable isotope geochemistry and petrography

The Fukuzaki seep deposit is composed of black, recrystallized carbonate matrix and micritic matrix, cut by veins filled with white sparry cements (Fig. 3b). The dominant mineral building the seep deposit is calcite (Table 1), varying in isotope composition from –40.2 ‰ to –37.2 ‰ for  $\delta^{13}\text{C}$  and from –14.4 ‰ to –12.2 ‰ for  $\delta^{18}\text{O}$  (Table 2). The most <sup>13</sup>C-depleted calcites are found in the recrystallized matrix ( $\delta^{13}\text{C}$  values of –37.2 ‰ and –40.2 ‰) and micrite (–36.8 ‰), while calcites forming sparry cements are much less <sup>13</sup>C-depleted ( $\delta^{13}\text{C}$  values of –12.9 ‰ and –12.6 ‰; Fig. 3c). The main non-carbonate mineral is quartz, followed by one or more clinopyroxenes: clinoenstatite, Fe enstatite, Mg ferrosillite, or pigeonite (Table 1). All these minerals were common near numerous pressure-dissolution features (Figs 3d, 4). Allochems found in the carbonate boulders comprise fossils: worm tubes (Fig. 3d) and shells (Fig. 4a), most likely of bivalve molluscs.

Volumetrically, the dominant phase is recrystallized matrix, composed of a mixture of cloudy and translucent spar, and largely euhedral blocky calcite (Fig. 4a). Micrite is also present, although in much smaller amounts (Fig. 3d). Both phases are penetrated by numerous pressure-solution seams, forming an interconnected network, lined by black opaque material (Fig. 4a). The seams often surround euhedral blocky calcite crystals (Fig. 4a, b), which have irregular faces, accentuated by opaque material, resulting most likely from accumulation of insoluble residues (Fig. 4a). The recrystallized matrix exhibits uniform dark orange luminescence, and is cut by bright orange luminescent microfractures visible only under CL imaging (Fig. 4b).

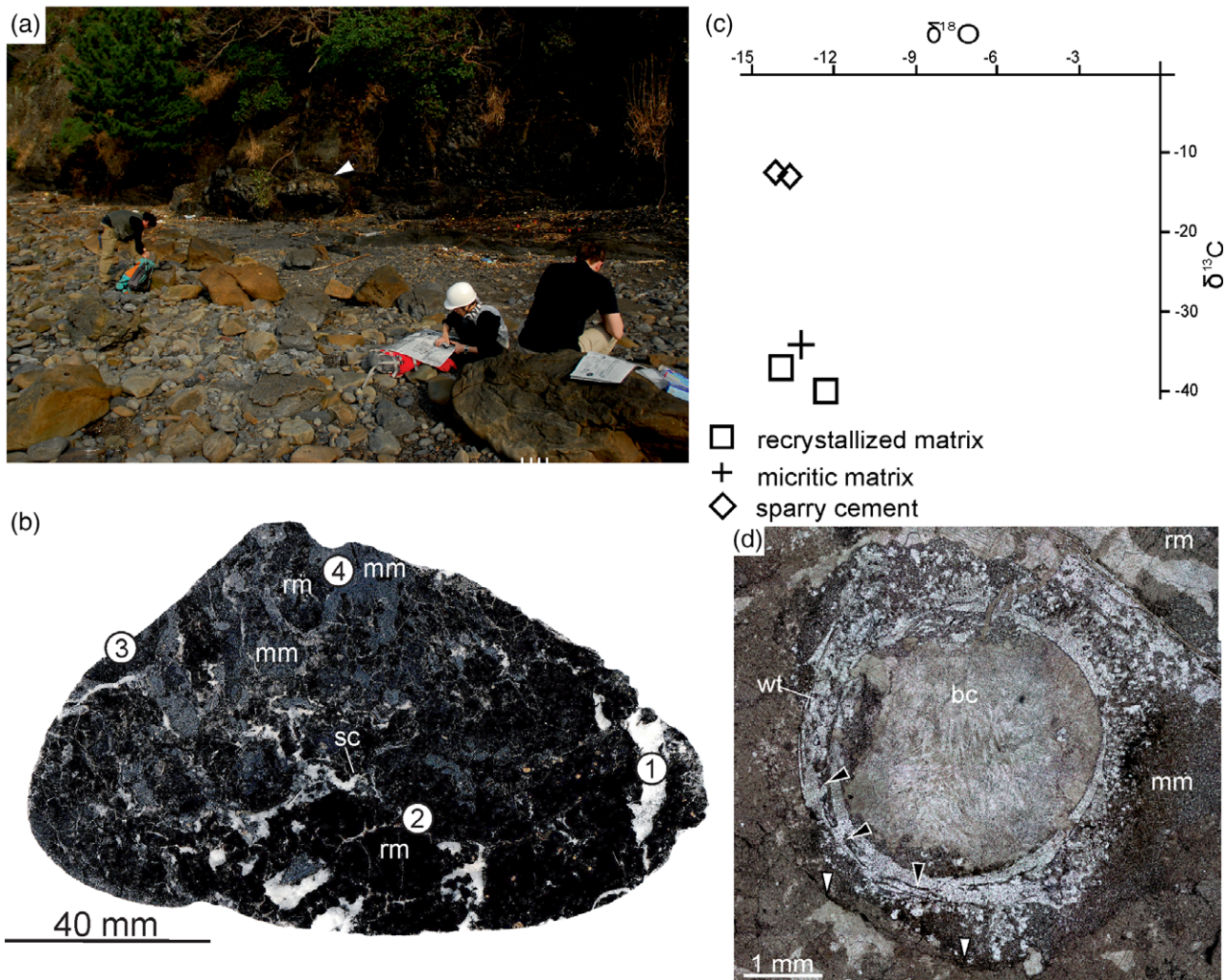


**Fig. 3.** (Colour online) Fukuzaki limestone. (a) Field photograph of the studied seep deposit. White arrow indicates carbonate body cropping out in the background; a large portion of material studied herein comes from the boulders visible in the foreground. Geologists for scale. (b) Polished slab of the Fukuzaki limestone: rm – recrystallized matrix, mm – micritic matrix, sc – sparry cements. Numbered points refer to location of samples studied with XRD (Table 1). (c) Cross-plot of  $\delta^{13}\text{C}$  and  $\delta^{18}\text{O}$  values of the Fukuzaki limestone. (d) Thin-section photomicrograph showing an agglutinated worm tube fossil (wt) with internally layered structure (black arrows); the worm tube is encapsulated in micritic matrix (mm) and filled with botryoidal cements (bc). Note pressure solution seam (white arrows) which affects the micritic matrix surrounding the worm tube, but does not affect the tube itself. Plane-polarized light.

#### 4.a.3. Organic geochemistry

Hydrocarbons were extracted from a carbonate mass of ~90 % recrystallized matrix and ~10 % sparry cements. Only minor amounts of hydrocarbons from the aliphatic hydrocarbon fractions were detected. These are mostly  $\text{C}_{17}$  to  $\text{C}_{19}$  and  $\text{C}_{23}$  to  $\text{C}_{31}$  *n*-alkanes, with unresolved complex mixture (UCM) around *n*- $\text{C}_{18}$  alkane. Total organic carbon content was below 0.1 wt % and its  $\delta^{13}\text{C}$  value was  $-42.3$  ‰.

#### 4.a.4. Macrofauna

Worm tubes have an outer diameter of 1.5 to 6 mm and a maximum observed length of *c.* 60 mm (Fig. 3d). All tubes are fairly straight, unbranched, occur as several tubes together rather than a dense cluster, and do not appear to be attached to substrate in the observed fragments. No outer wall ornamentation is discernible, and it is also not possible to determine if the tubes taper along their length. In thin-section, tube walls are 0.5–1 mm in thickness, and contain a thick outer layer of fine-grained sediment. Towards the inside of the tube wall, fine disintegrated layers are present. In one of the tubes, these interrupted layers

occur throughout the tube wall where they are mixed with varying amounts of sediment (Fig. 3d). These tubes appear to have originally been agglutinated, and thus composed of sediment mixed with organic secretions that are used to adhere sediment to the tube (Merz, 2015). Such tubes generally have a structure of greater amounts of sediment towards the outer tube wall, while the inside of the tube wall is lined with organic layers (Georgieva *et al.* 2019). Various marine animals such as annelids and crustaceans may construct agglutinated tubes; however, the diameter and length of these tubes is perhaps most consistent with having been made by an annelid. Annelids which build similarly sized agglutinated tubes include sabellids, terebellids, ampharctids and maldanids.

Apart from the worm tubes, the macrofauna of the Fukuzaki limestone comprise a species of mytilid, up to 41.5 mm long and 22.5 mm high with an H/L ratio of 0.54 (Fig. 5). The species from Fukuzaki was previously identified as *Bathymodiolus* sp. by Ninomiya (2011) and Ninomiya *et al.* (2020). It has a moderately elongated shell with a small, elongated anterior adductor muscle scar, small anterior and larger posterior lobe and edentulous dorsal

**Table 1.** Mineral composition of selected facies from the Taishu Group seep deposits described in this study. For XRD diagrams, see Supplementary Material available online at <https://doi.org/10.1017/S001675682000103X>

Deposit	Sample	Facies	Mineral assemblage
Fukuzaki			
	1	Vein-filling sparry cement	Calcite, quartz
	2	Recrystallized matrix with stylolite	Calcite and quartz, minor amounts of clinopyroxene (Mg ferrosillite, Fe enstatite, pigeonite or clinoenstatite)
	3	Recrystallized matrix	Calcite, quartz
	4	Micritic matrix	Calcite and quartz, possibly clinopyroxene (enstatite)
Kanoura			
	1	Bivalve-filling radial fibrous cement	Calcite, minor amounts of quartz
	2	Bivalve-filling recrystallized matrix	Calcite, quartz and ankerite
	3	Void-filling recrystallized matrix 2	Calcite, quartz and ankerite
	4	Bivalve-filling recrystallized matrix 1	Calcite, quartz
	5	Micritic matrix	Calcite, quartz
Tanohama			
	1	Radial fibrous cement (void-filling, concretionary facies)	Calcite, quartz
	2	Recrystallized matrix (concretionary facies)	Calcite, quartz
	3	Internal sediment (concretionary facies)	Quartz, ankerite, chalkopyrite and/or pyroxene and/or clinoenstatite
	4	Nodule (stromatolitic facies)	Calcite, quartz
	5	Internal sediment (stromatolitic facies)	Quartz, calcite and dolomite
	6	Base of stromatolitic crust (stromatolitic facies)	Calcite, quartz
	7	Centre of stromatolitic crust (stromatolitic facies)	Calcite

margin and is hereby identified as '*Bathymodiolus akanudaensis*' (Kuroda, 1931). The species has previously been reported from the middle Miocene Akanuda and Anazawa seep deposits from the Bessho Formation, Nagano Prefecture, Japan (Tanaka, 1959; Miyajima *et al.* 2017), from the latest middle Miocene Kita-Kuroiwa seep deposits from the Ogaya Formation, Niigata Prefecture, Japan (Amano *et al.* 2010), and from the late Miocene Nakanomata seep deposit from the Nodani Formation, Niigata Prefecture, Japan (Miyajima *et al.* 2016). We hereby agree that the species from Fukuzaki is conspecific with '*B.*' *akanudaensis*. However, due to a lack of taxonomically important byssal muscle scars preserved in any of the '*B.*' *akanudaensis* specimens that we examined (cf. Cosel & Janssen, 2008; Saether *et al.* 2010b; Amano & Jenkins, 2011b; Xu *et al.* 2019), we are unable to resolve the generic identity of this species.

#### 4.b. Kanoura limestone

##### 4.b.1. Locality description

The Kanoura seep deposit represents a set of boulders found on Kamishima, c. 4 km north of Minechosaka Town. Access to the site is through prefectural road 39 north of Minechosaka Town towards Minechoshitaka Town (Fig. 1) and turning east into an unnamed asphalt road prior to the first tunnel. The deposit consists of loose blocks, which have fallen from the slope south of the pier at 34° 28' 16.86" N, 129° 23' 36.96" E (Fig. 6a); the blocks are composed of moderately hard, brittle grey carbonate.

##### 4.b.2. Mineralogy, stable isotope geochemistry and petrography

The Kanoura seep deposit is composed of grey, recrystallized matrix with yellow microspar filling the voids or bivalve shells (Fig. 6b). The XRD pattern indicates that the dominant mineral forming the carbonate is calcite (Table 1), with  $\delta^{13}\text{C}$  values ranging from  $-41.8\text{‰}$  to  $-19.9\text{‰}$  and  $\delta^{18}\text{O}$  values from  $-14.5\text{‰}$  to  $-10.4\text{‰}$  (Table 2). The most  $^{13}\text{C}$ -depleted calcites are those building radial cements ( $\delta^{13}\text{C}$  values from  $-41.8\text{‰}$  to  $-41.0\text{‰}$ ), while the recrystallized matrix is considerably less depleted and shows more scattered  $\delta^{13}\text{C}$  values (from  $-30.7\text{‰}$  to  $-19.9\text{‰}$ ; Fig. 6c). The other carbonate mineral is identified as ankerite, which together with calcite and quartz forms yellow microspar filling voids and bivalve shells ( $\delta^{13}\text{C}$  values from  $-19.5\text{‰}$  to  $-7.1\text{‰}$ ). Non-carbonate minerals comprise quartz and trace amounts of unidentified clinopyroxene (Table 1). The carbonate contains numerous fossils, chiefly planktonic foraminifera (Fig. 7a) and vesicomid bivalve shells.

The recrystallized matrix is composed of a mixture of cloudy and translucent calcite spar, cut by pressure-dissolution seams (Fig. 7a). The matrix contains enclaves of micrite, preserved either as nodules (Fig. 7b) or patches adjacent to bivalve shells and cement-filled cavities (Fig. 7c). Cavities, whether inside bivalve shells or within the matrix itself, are filled with yellow microspar composed of subhedral calcite and ankerite crystals with minor amounts of detrital quartz (Table 1; Fig. 7b, c). The yellow microspar occasionally forms distorted geopetals (Fig. 7c). The

**Table 2.** Stable carbon and oxygen isotopic compositions of the Taishu Group seep deposits described in this study

Deposit	Sample	Facies	$\delta^{13}\text{C}$ (‰)	$\delta^{18}\text{O}$ (‰)
Fukuzaki	fs01	recrystallized matrix	-37.2	-14.0
	fs02	sparry cement	-12.6	-14.4
	fs04	sparry cement	-12.9	-13.8
	fs05	recrystallized matrix	-40.2	-12.2
	Fuk 2/1	micritic matrix	-36.8	-13.2
Kanoura	ku01	recrystallized matrix	-25.1	-14.0
	ku02	radial cement	-41.1	-11.8
	ku03	recrystallized matrix	-30.7	-14.9
	ku04	recrystallized matrix	-19.9	-14.0
	ku07	radial cement	-41.8	-10.4
	ku08	radial cement	-41.0	-12.2
	Kan 1/2	yellow microspar, bivalve-filling	-7.1	-9.7
	Kan 2/2	yellow microspar, cavity-filling	-19.5	-11.12
Tanohama	tn02	sparry cement	-8.2	-13.8
	tn04	sparry cement	-17.8	-13.1
	tn05	shell	-4.7	-4.6
	tn06	micritic matrix	-15.3	-13.3
	tn07	radial cement	-50.5	-2.4
	tn08	micritic matrix	-26.5	-12.6
	tn09	sparry cement	-48.2	-2.2
	tn10	yellow calcite	-32.3	-2.2
	tn11	radial cement	-45.2	-5.0
	tn12	sparry cement	-46.3	-3.5
	tn13	sparry cement	-17.3	-13.4
	tn14	micritic matrix	-17.9	-13.3
	tn15	shell	-32.4	-8.4
	tn17	sparry cement	-13.6	-13.4
	tn18	sparry cement	-52.8	-2.4
	tn19	yellow calcite	-41.0	-5.9
	tn20	sparry cement	-49.6	-4.4
	tn21	radial cement	-49.0	-4.8
	Tan 1/2	micritic matrix, nodule	-22.9	-12.4
	Tan 2/2	micritic matrix, nodule	-23.4	-12.6

remaining volume of the cavities, where present, is filled with bladed cements and equant calcite spar (Fig. 7c).

Radial cements are encased in micrite (Fig. 7d) or cover bivalve shell surfaces. All cements observed were recrystallized, and we were unable to observe the crystallite morphology under optical microscopy. CL microscopy reveals that marginal parts of the cement crusts show orange luminescence, and fibrous enclaves within the crust show dark to no luminescence

(Fig. 7d). Micrites hosting the cements show variable luminescence, with micrite generations at the base of the crust being usually more luminescent than those post-dating the crust (Fig. 7d).

#### 4.b.3. Organic geochemistry

Hydrocarbons were extracted from a carbonate mass of ~80 % recrystallized matrix and ~20 % radial cements. As in the case of Fukuzaki, only minor amounts of  $\text{C}_{17}$  to  $\text{C}_{19}$  and  $\text{C}_{23}$  to  $\text{C}_{31}$  *n*-alkanes were detected at Kanoura, with unresolved complex mixture (UCM) around *n*- $\text{C}_{18}$  alkane. Total organic carbon content was below 0.1 wt % and its  $\delta^{13}\text{C}$  value was -35.6 ‰.

#### 4.b.4. Macrofauna

The only macrofaunal species found in the Kanoura limestone is an elongated vesicomid bivalve (Fig. 8). Bivalves from the Kanoura locality have previously been interpreted as belonging to at least two species of the vesicomid *Calyptogena* Dall, 1891, occurring in both the seep limestone and surrounding mudstone, and an additional species of the mytilid *Adipicola* Dautzenberg, 1927, occurring only in the surrounding mudstone (Ninomiya, 2011). Our observations indicate that at least the materials from the Kanoura carbonate belong to a single species. The largest complete specimen at our disposal is 48.5 mm long and 16.5 mm high, with a H/L ratio of *c.* 0.34. The elongated shape and pallial line emerging at the posterior side of the anterior adductor muscle scar places the species in the genus *Pleurophopsis* Van Winkle, 1919 (Kiel, 2007; Krylova *et al.* 2010), a senior synonym of *Adulomya* Kuroda, 1931 (Amano & Kiel, 2011; Amano *et al.* 2019a). Morphologically, the species is most similar to *Pleurophopsis chitanii* (Kanehara, 1937), known from early to middle Miocene localities on both the Sea of Japan and Pacific sides of Japan (Amano & Kiel, 2011; Amano *et al.* 2019a, b). Many specimens from Kanoura are deformed, with the posterior lobe squeezed into the remainder of the shell, which gives an impression of a false deep ventral sinus (Fig. 8a–b; Ninomiya, 2011, p. 4, figs 5–6). However, undeformed shells have straight to slightly concave ventral margins (Fig. 8c–i) known in *P. chitanii*. The posterior portion of the pallial line is formed by a series of muscle attachments and bends sharply upward (Fig. 8f); however, the portion of the pallial line where the false sinus is developed in *P. chitanii* is not preserved, and we are unable to verify the presence of this feature. Nonetheless, based on the observed morphological features, such as the H/L ratio, shape of the ventral margin and size of the anterior lobe, the species can be safely included into *Pleurophopsis chitanii* (Kanehara, 1937).

#### 4.c. Tanohama limestone

##### 4.c.1. Locality description

The Tanohama seep deposit was found *c.* 700 m north of the fishing town of Kamiagatamachi Shitaru (Fig. 1). The easiest way to access it is to follow the cliff northwards from the harbour, preferably during low tide. In 2016 the deposit was preserved *in situ* a few metres above the base of the cliff at 34° 34' 32.34" N, 129° 17' 49.44" E. The deposit is composed of a ~3.7 m long and ~1 m thick *in situ* carbonate body and centimetre-sized concretions scattered in siltstone both above and below the carbonate body. There is an additional, smaller carbonate body a few metres above the main deposit. A pipe-shaped concretion is also found below the main carbonate (Fig. 9a). This seep deposit is formed of concretionary, micritic and stromatolitic carbonates (Fig. 9b).

**Fig. 4.** (Colour online) Fukuzaki limestone. (a) Thin-section photographs showing recrystallized matrix (rm) of Fukuzaki limestone yielding numerous pressure-solution seams (white arrows) and a recrystallized bivalve shell (sh). Cross-polarized light image. (b) Thin-section photographs showing heavily recrystallized matrix cross-cut by pressure-solution seams (white arrows). Most of the recrystallized matrix exhibits dark orange luminescence, with bright orange luminescence seen in microfractures (black arrow). Cathodoluminescence image.

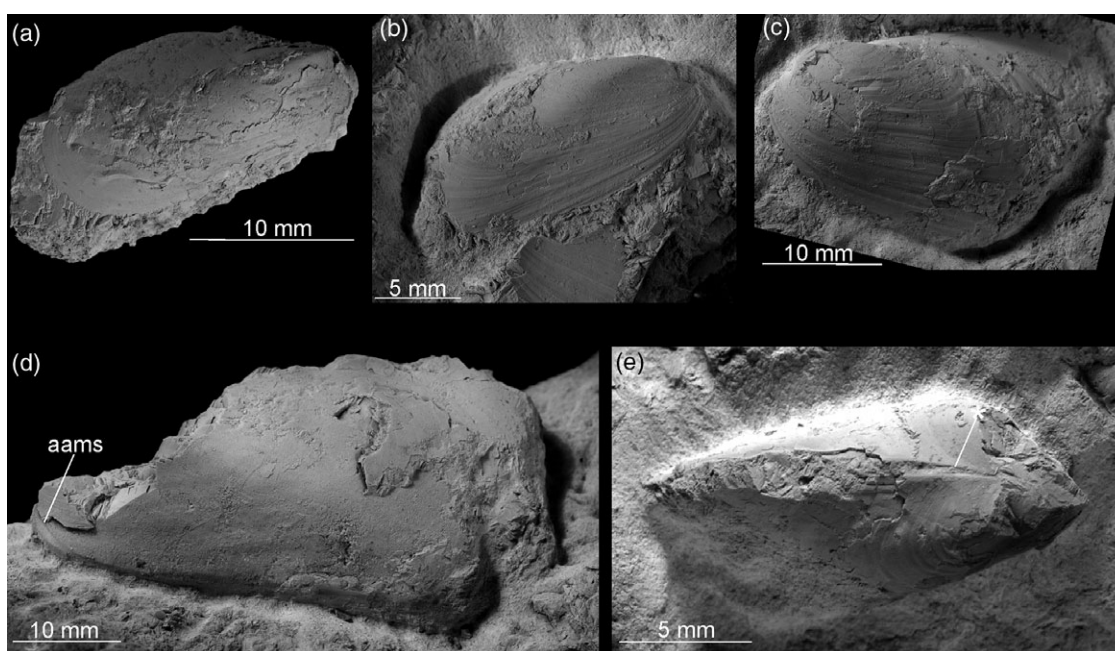
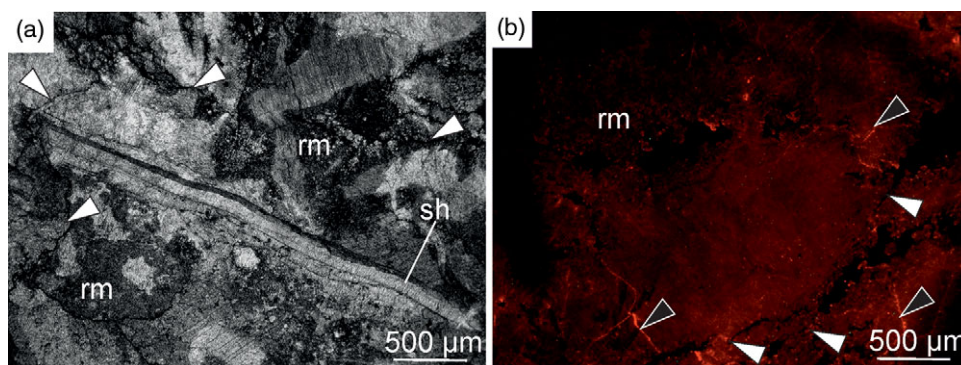


**Fig. 5.** *Bathymodiolus akanudaensis* (Kuroda, 1931) from the Fukuzaki limestone. (a) Right-lateral view of a complete specimen. Shell. ZPAL V.55/1. (b) Right-lateral view of an incomplete specimen. Partial shell. ZPAL V.55/2. (c) Left-lateral view of an incomplete specimen. Shell. ZPAL V.55/3. (d) Left-lateral view of a damaged specimen, with the anterior adductor muscle scar (aams) indicated. Internal mould with fragments of shell adhering. ZPAL V.55/4. (e) Dorsal view of an incomplete specimen, with the edentulous dorsal margin indicated (asterisk). Partial shell. ZPAL V.55/5.

#### 4.c.2. Mineralogy, stable isotope geochemistry and petrography

The Tanohama seep deposit is composed of nodular, yellowish-grey micritic matrix intercalated with stromatolitic crusts composed of radiaxial cements, the latter also filling smaller voids within the micritic and recrystallized matrix. The XRD pattern indicates that the bulk of the carbonate is calcite (Table 1), with  $\delta^{13}\text{C}$  values ranging from  $-52.8\text{‰}$  to  $-4.7\text{‰}$  and  $\delta^{18}\text{O}$  values from  $-13.8\text{‰}$  to  $-2.2\text{‰}$  (Fig. 9c; Table 2). Most  $^{13}\text{C}$ -depleted are the calcites building radiaxial cements ( $\delta^{13}\text{C}$  values between  $-52.8\text{‰}$  and  $-45.2\text{‰}$ ), followed by yellow calcites ( $\delta^{13}\text{C}$  values from  $-41.0\text{‰}$  to  $-32.3\text{‰}$ ), bivalve shells ( $\delta^{13}\text{C}$  values from  $-32.4\text{‰}$  to  $-4.7\text{‰}$ ), micrite, in the form of both homogeneous micrite ( $\delta^{13}\text{C}$  values from  $-26.5\text{‰}$  to  $-15.3\text{‰}$ ) and nodules ( $\delta^{13}\text{C}$  values from  $-23.4\text{‰}$  to  $-22.9\text{‰}$ ), and blocky cements ( $\delta^{13}\text{C}$  values from  $-17.3\text{‰}$  to  $-8.2\text{‰}$ ). Other carbonate minerals are dolomite and ankerite, found in minor amounts in sediment trapped between the growing nodules (Fig. 9d–e; Table 1). Non-carbonate minerals comprise quartz, chalcopyrite and clinopyroxenes, found chiefly in the internal sediment or as

small impurities within carbonate-rich phases (Table 1). The carbonate contains fossils such as planktonic foraminifers (Fig. 10a) and vesicomid bivalve shells (Fig. 10b).

The micritic matrix forming the bulk of the carbonate is cut by numerous pressure-dissolution seams accentuated by dark, insoluble residue (Fig. 10b). Some cavities in the micrite are lined with clotted carbonate, composed of cloudy micritic clots up to  $100\text{ }\mu\text{m}$  across, interlayered with radiaxial cement (Fig. 10c). Other cavities are lined with an irregular layer of yellow calcite, followed by recrystallized radiaxial cements with noticeable traces of a fibrous precursor and characteristic flat-topped or needle-like terminations (Fig. 10d). Radiaxial cements and micrites from Tanohama are predominantly non-luminescent; only a thin veneer of micrite immediately below the radiaxial cement crust displays orange luminescence (Fig. 10e–f).

The top of the main Tanohama seep deposit (Fig. 9b) is composed of accumulation of micritic carbonate nodules (Figs 9e and 11a), covered with a cement crust up to  $c. 100\text{ mm}$  in thickness (Fig. 9b, e). The nodules are up to  $c. 15\text{ mm}$  in diameter and are



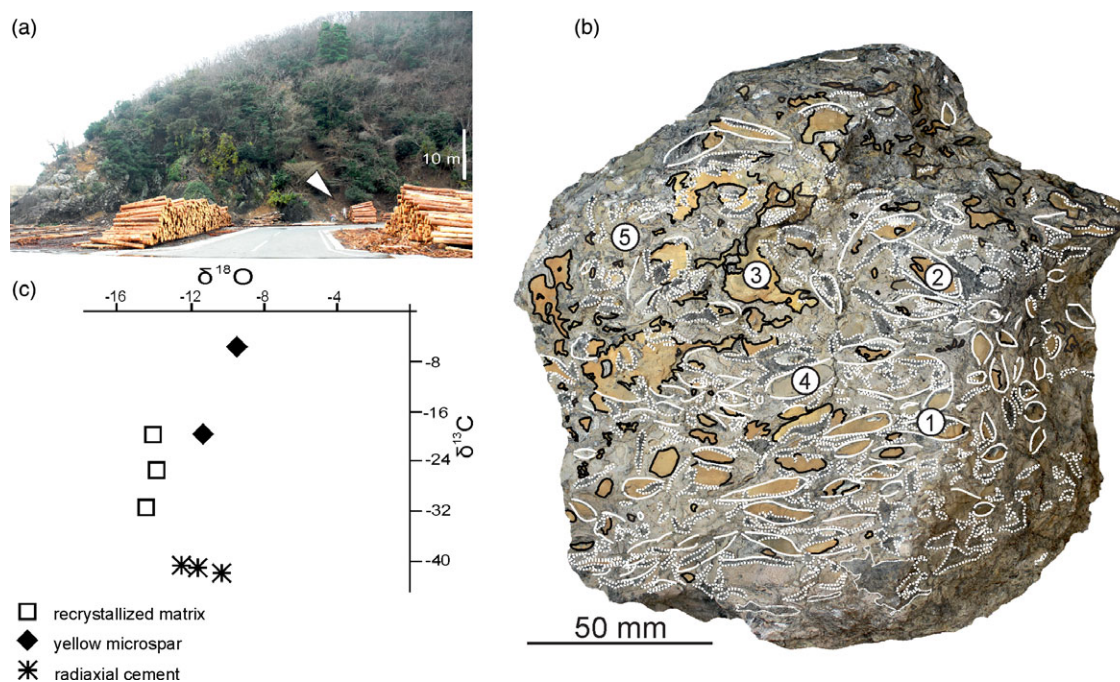


**Fig. 6.** (Colour online) Kanoura limestone. (a) Field photograph of the study site. White arrow indicates fragments of the seep deposit preserved as boulders in the scree. (b) Weathered surface of a seep deposit block showing carbonate textures; solid white lines indicate the observed vesicomid bivalve shells; stippled white lines – radiaxial cements; black lines – yellow microspar filling voids. Numbers correspond to carbonate samples for XRD study from a corresponding polished slab (Table 1). (c) Cross-plot of  $\delta^{13}\text{C}$  and  $\delta^{18}\text{O}$  values of the Kanoura limestone (‰).

composed of layered (Fig. 9e) or homogeneous (Fig. 11a) micrite. The space between the nodules is partially filled by internal sediment which can be cut by pressure-dissolution seams affecting only the internal sediment and not the nodules (Fig. 11a). Cavities between internal sediment and nodules, where present, are occluded by recrystallized radiaxial cements, nucleating at the surface of nodules; some of those radiaxial cements show traces of a fibrous precursor (Fig. 11b–c). A thick stromatolitic crust composed of radiaxial cements covers the corrosion surface truncating nodules and internal sediment, either pristine or fractured (Fig. 9e). The surface is followed either directly by radiaxial cements (Figs 11c) or by a sequence of yellow calcites and radiaxial cements (Fig. 11d). The latter pattern can be repeated several times within the crust. Radiaxial fibrous cements are uniformly recrystallized; ghosts of a fibrous precursor are, however, visible (Fig. 11d). Other precipitates include subhedral dolomite occasionally formed between the nodules within the internal sediment (Fig. 11e), and silica (chalcedony and anhedral quartz) formed in the few radially arranged cavities found within radiaxial cement crust (Fig. 11f).

#### 4.c.3. Organic geochemistry

Hydrocarbons were extracted from the concretionary facies (~50 % micrite and ~50 % sparry cements) and the stromatolitic facies (100 % radiaxial cements). Both subsamples have remarkably similar hydrocarbon composition, dominated by  $\text{C}_{14}$  to  $\text{C}_{28}$  *n*-alkanes. The extracted *n*-alkanes clearly show a short-chain predominance, with lower abundance with increasing carbon number. Isoprenoid hydrocarbons, such as crocetane and pentamethylcosane (PMI), were not detected, except for minor amounts of pristane and phytane in the stromatolitic facies (Fig. 12). Steranes and hopanes were also undetectable. Hydrocarbons extracted from the stromatolitic facies after carbonate dissolution by HCl did not show any

compositional difference from those extracted without carbonate dissolution. Total organic carbon content of the stromatolitic facies was ~0.1 wt % and its  $\delta^{13}\text{C}$  value was very low (–48.9 ‰).

#### 4.c.4. Macrofauna

The macrofauna from the Tanohama limestone comprises four species (Fig. 13). The most common is a vesicomid bivalve species, previously interpreted as belonging to two unnamed species of *Calyptogena* occurring also at the Kanoura locality (Ninomiya, 2011). The species has a moderately elongated shell up to 34 mm long and 15 mm high, with an H/L ratio of *c.* 0.44. This is within the range of elongation of similarly sized specimens of *Pleurophopsis hamuroi* (Amano & Kiel, 2011) and *P. kuroiwaensis* (Amano & Kiel, 2011). The beak is positioned in the anterior one-fourth to one-seventh of the shell, more similar to its position in adult specimens of *P. hamuroi* than that of *P. kuroiwaensis* (Amano & Kiel, 2011). The species from Tanohama is significantly inflated, in which it resembles *P. hamuroi* rather than *P. kuroiwaensis*, and has a cardinal dentition with small 2a cardinal. Based on the above criteria, we identify the vesicomid species from Tanohama into *Pleurophopsis cf. hamuroi* (Amano & Kiel, 2011).

Other macrofaunal species are much less common in Tanohama. They include a species of the lucinid bivalve *Lucinoma* Dall, 1901. Numerous species of *Lucinoma* have previously been reported from the Miocene seep deposits from the Northern Pacific area (cf. Majima *et al.* 2005), and we refrain from including *Lucinoma* from Tanohama into any of these until a thorough revision is available as suggested by Kiel (2013). The remaining materials comprise a single specimen of the mytilid bivalve '*Bathymodiolus akanudaensis*' (Kuroda, 1931), and three poorly preserved gastropod specimens, possibly of *Provanna* Dall, 1918 (e.g. Amano & Little, 2014).

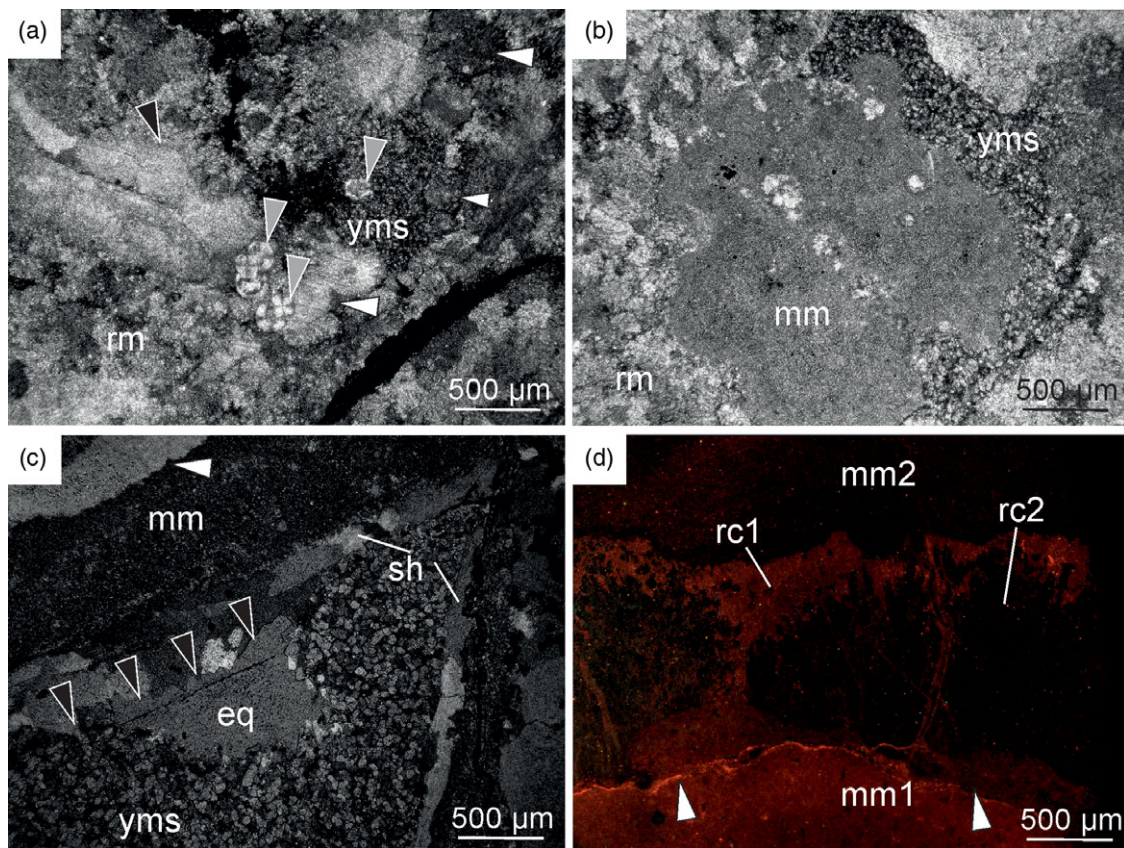


**Fig. 7.** (Colour online) Kanoura limestone. (a) Thin-section photomicrographs showing recrystallized matrix (rm) of the Kanoura limestone with pressure-solution seam (white arrows) and planktonic foraminifera (grey arrows). Yellow microspar (yms) fills small cavity in the recrystallized matrix. Cross-polarized light image. (b) Thin-section photomicrographs showing nodule of micrite (mm) surrounded by recrystallized matrix (rm) and yellow microspar (yms). Cross-polarized light image. (c) Thin-section photomicrographs showing a recrystallized vesicomid bivalve shell (sh) encapsulated in micritic matrix (mm) and filled with yellow microspar (yms) and equant spar (eq). Black arrows mark the surface of bladed cements, rimming the matrix-free interior of the bivalve shell. Note that there is only a thin veneer of micritic matrix on the outer surface of shell, accompanied by a cement-filled cavity (white arrow). Cross-polarized light image. (d) Thin-section photographs showing radiaxial cements (rc) encapsulated in micritic matrix (mm1 and mm2). Micritic matrix predating the radiaxial cements (mm1) shows dark orange luminescence, and the micritic matrix covering the crust (mm2) shows dull to no luminescence. Radiaxial cements show orange luminescence (rc1), apart from enclaves inside the cement crust which show dark to no luminescence (rc2). Micritic matrix is cut by a pressure-solution seam (white arrow). Cathodoluminescence image.

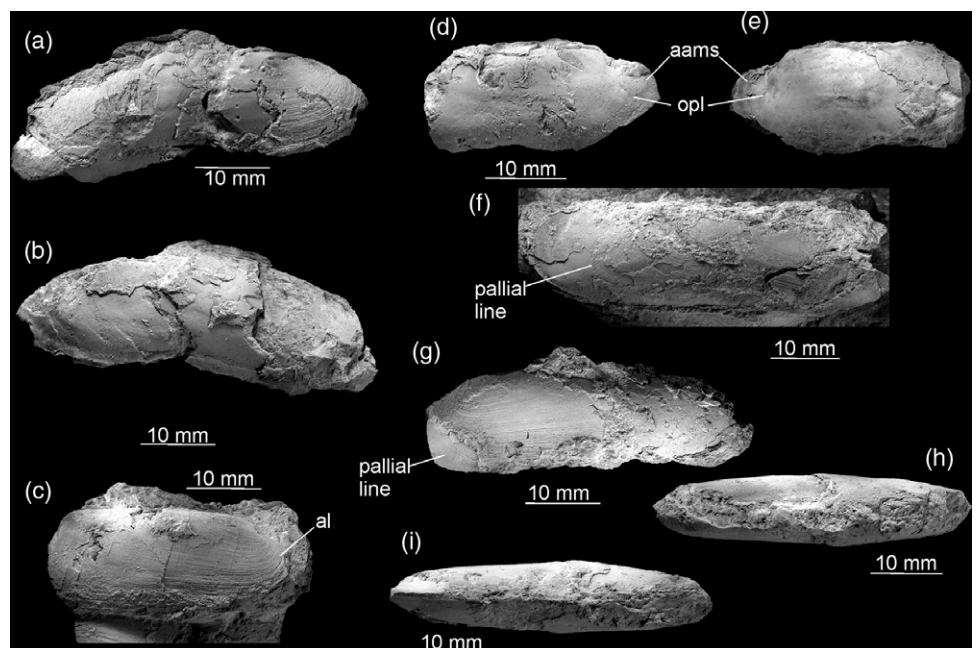


**Fig. 8.** *Pleurophopsis chitani* (Kanehara, 1937) from the Kanoura limestone. (a–b) Right- (a) and left- (b) lateral views of a complete, deformed specimen with false ventral sinus formed by broken valves. Internal mould with adhering fragments of the shell. ZPAL V. 55/6. (c) Right-lateral view of the anterior part of an incomplete right valve with the anterior lobe (al) indicated. Partial shell. ZPAL V. 55/7. (d–e) Right- (d) and left- (e) lateral views of an incomplete specimen with anterior adductor muscle scars (aams) and point of origination of the pallial line (opl) visible. Internal mould. ZPAL V.55/8. (f) Right-lateral view of an incomplete specimen with the pallial line forming a weak sinus. Internal mould with adhering fragments of the shell. ZPAL V.55/9. (g–i) Left-lateral (g), dorsal (h) and ventral (i) views of a nearly complete specimen. Partial shell. ZPAL V.55/10.

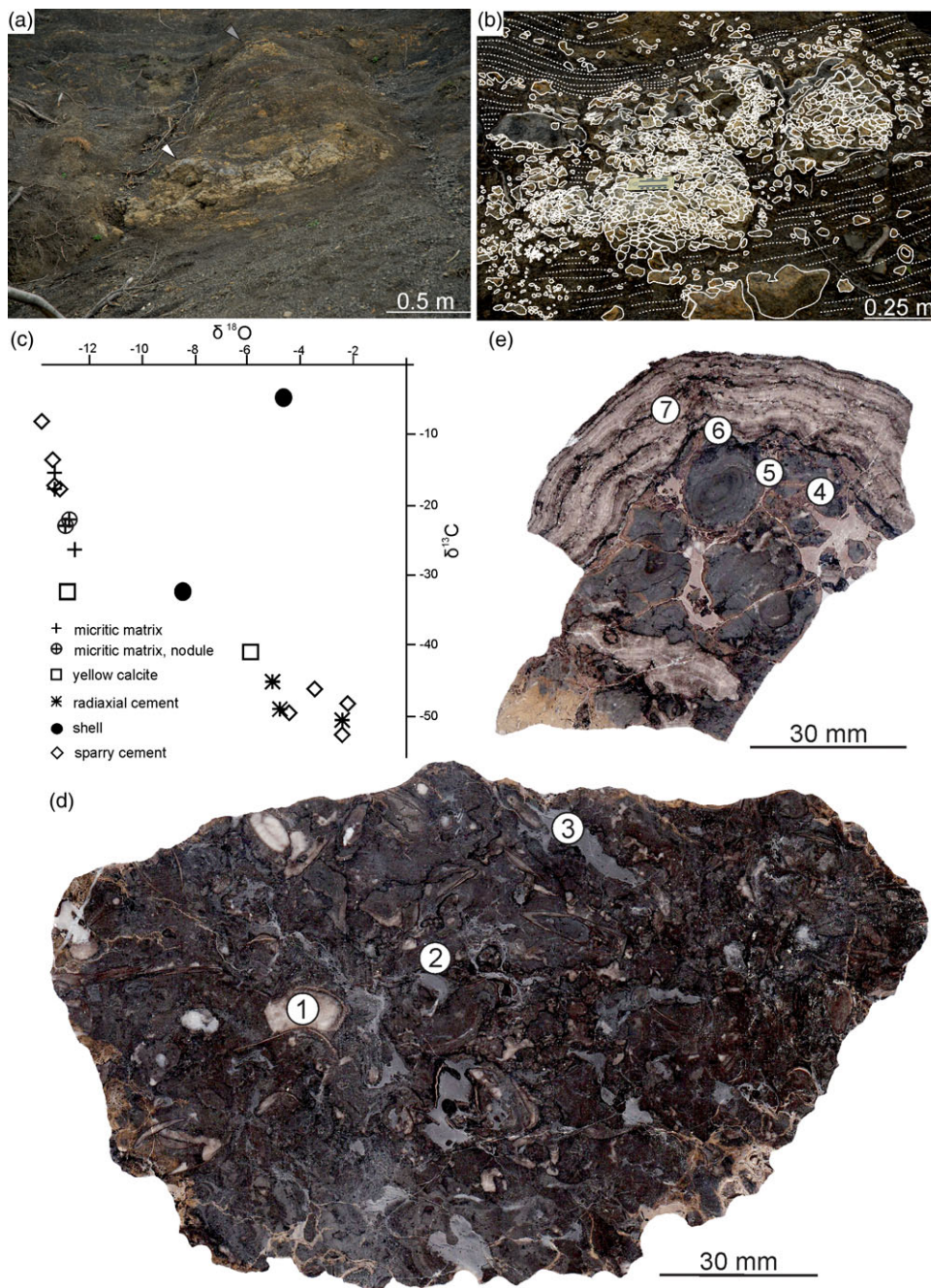


**Fig. 9.** (Colour online) Concretionary facies of the Tanohama limestone. (a) Field photograph of a studied seep deposit. White arrow marks lower seep deposit. Grey arrow marks smaller, upper seep deposits a few metres above the lower seep deposit. The majority of Tanohama limestone material studied comes from the lower seep deposit. (b) Distribution of carbonate bodies comprising the lower seep deposit at Tanohama. White solid lines delineate major concretions that we were able to track in the field and on the photographs; white dotted lines delineate stromatolitic crusts; white stippled lines indicate host sediment bedding. (c) Cross-plot of  $\delta^{13}\text{C}$  and  $\delta^{18}\text{O}$  values of the Tanohama limestone (‰). (d) Polished slab of the concretionary facies of the Tanohama limestone; numbered points refer to locations of samples studied with XRD (Table 1). (e) Polished slab of stromatolitic facies of Tanohama limestone; numbered points refer to location of samples studied with XRD (Table 1).

## 4. Interpretations

### 5.a. Miocene methane seepage within the Taishu Group

Two lines of evidence unequivocally show that the Miocene authigenic carbonate deposits found within the Taishu Group formed at submarine methane seeps. These are (i) the strong  $^{13}\text{C}$  depletion of their carbonate minerals, and (ii) petrography of the most  $^{13}\text{C}$ -depleted carbonate phases.

All three studied deposits exhibit low  $\delta^{13}\text{C}$  values of calcites, ranging from  $-40.2$  ‰ to  $-12.6$  ‰ (Fukuzaki),  $-41.8$  ‰ to  $-19.9$  ‰ (Kanoura) and  $-52.8$  ‰ to  $-4.7$  ‰ (Tanohama). The majority of those values point to a carbon source isotopically much lighter than ambient-seawater dissolved inorganic carbon ( $c. -2$  to

$+2$  ‰ VPDB) and carbon coming from degradation of sedimentary organic matter ( $c. -25$  ‰ to  $-20$  ‰ VPDB; Krajewski & Luks, 2003; Campbell, 2006). The low  $\delta^{13}\text{C}$  values encountered in the carbonates from the Taishu Group are consistent with hydrocarbons being the primary source of carbon incorporated into the studied authigenic carbonates (Peckmann & Thiel, 2004; Campbell, 2006). The most abundant hydrocarbon in marine pore fluids is methane (Whiticar, 1999), and microbially mediated anaerobic oxidation of methane (AOM; Boetius *et al.* 2000) releases bicarbonate anions and in consequence facilitates precipitation of authigenic carbonate minerals (Peckmann & Thiel, 2004). Aerobic oxidation of methane, on the other hand, increases the acidity and thus causes carbonate dissolution, rather than

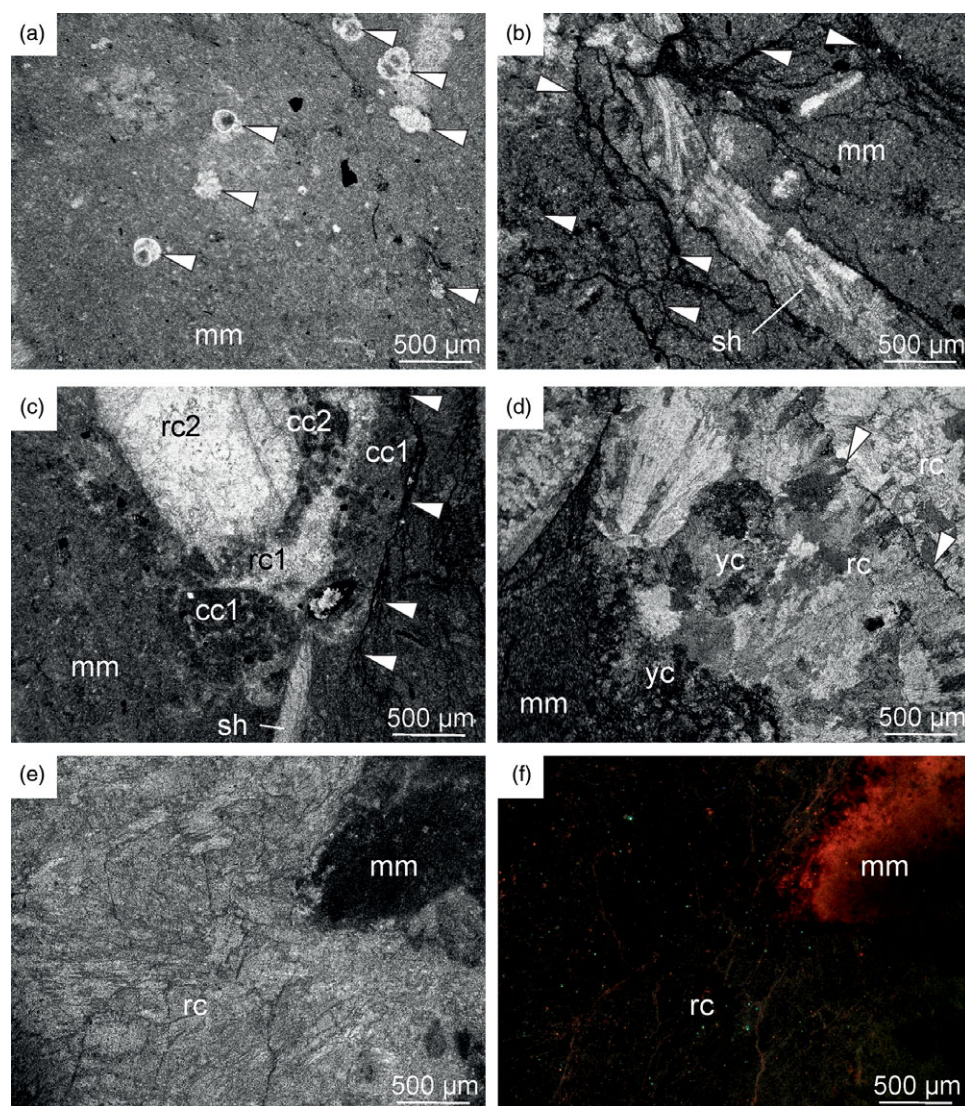


**Fig. 10.** (Colour online) Concretionary facies of the Tanohama limestone. (a) Thin-section photomicrograph showing micritic matrix (mm) yielding several planktonic foraminifera (white arrows). Plane-polarized light. (b) Thin-section photomicrograph showing micritic matrix (mm) with the vesicomid bivalve shell (sh) and numerous pressure-solution seams penetrating the matrix in the immediate vicinity of the shell (white arrows). Cross-polarized light image. (c) Thin-section photomicrograph showing a cavity within micritic matrix (mm) lined with at least two generations of clotted carbonate (cc1 and cc2) and filled with two subsequent generations of radiaxial cements (rc1 and rc2). Plane-polarized light image. (d) Thin-section photomicrographs showing a cavity within micritic matrix (mm) filled with yellow cements (yc) and radiaxial cements (rc). White arrows indicate the surface of radiaxial cement crust with needle to flat-topped crystal terminations. Cross-polarized light image. (e–f) Thin-section photomicrographs showing a contact between micritic matrix (mm) and radiaxial cement (rc). Micritic matrix zone adjacent to the base of the radiaxial cement crust shows dark orange luminescence, and the subsequent cement shows no luminescence. Plane-polarized light (e) and cathodoluminescence image (f).

precipitation (Himmler *et al.* 2011). In addition, much less common, heavier gaseous hydrocarbons and oils are also oxidized in marine environments (e.g. Joye *et al.* 2004; Smrzka *et al.* 2019); however, their contribution to the overall carbonate pool at seeps remains poorly understood. Consequently, significantly  $^{13}\text{C}$ -depleted values of the Miocene authigenic carbonates from the Taishu Group indicate that methane-derived carbonate released during AOM was involved in their formation (cf. Peckmann & Thiel, 2004). The methane involved could have been either biogenic ( $\delta^{13}\text{C}$  below  $-50$  ‰ VPDB) or thermogenic in origin ( $-30$  ‰ to  $-50$  ‰ VPDB; Whiticar, 1999; Campbell, 2006). Assuming a certain degree of mixing of different carbonate pools that always takes place at seeps (e.g. Peckmann & Thiel, 2004; Kiel & Peckmann, 2007; Peckmann *et al.* 2009), and that the low  $\delta^{13}\text{C}$  values of carbonate are closest to those of the original hydrocarbon source (e.g. Peckmann *et al.* 2011; Himmler *et al.* 2015), the  $\delta^{13}\text{C}$  values of  $-40.2$  ‰ for Fukuzaki,  $-41.8$  ‰ for Kanoura and  $-52.8$  ‰ for Tanohama indicate that all three deposits formed due to seepage of biogenic methane (e.g. Hryniewicz *et al.* 2016; Miyajima *et al.* 2016, 2018). Nevertheless, we cannot exclude that thermogenic methane or heavier hydrocarbons could also have contributed to the overall carbon budget.

Because of the pervasive recrystallization that obliterated most of the primary fabrics, no seep-specific textures have been preserved in the Fukuzaki limestone (Fig. 4). However, features typical for carbonates formed at methane seeps are present at Kanoura and Tanohama. The micritic matrix of the Kanoura and Tanohama limestones, whether partially recrystallized in the case of Kanoura or purely micritic in the case of Tanohama, contains cavities filled with radiaxial cements (Figs 7, 10 and 11). At Kanoura, only remnants of the original radiaxial textures are preserved, as shown by CL imaging (Fig. 7d). At Tanohama, radiaxial cements preserve their original fibrous textures, in spite of later recrystallization (Figs 10d–f and 11b–d). Notably, radiaxial cements are the most  $^{13}\text{C}$ -depleted phases at both Kanoura ( $-41.8$  ‰ to  $-41.0$  ‰) and Tanohama ( $-52.8$  ‰ to  $-45.2$  ‰).  $^{13}\text{C}$ -depleted radiaxial cements are typical for hydrocarbon seeps, both ancient and Recent (e.g. Savard *et al.* 1996; Campbell *et al.* 2002; Greinert *et al.* 2002; Campbell, 2006; Feng *et al.* 2010; Hammer *et al.* 2011; Jakubowicz *et al.* 2015), and their presence in both Kanoura and Tanohama further corroborates the seep-related origin of both deposits. The fibrous morphology of cements at Tanohama is paired with an aragonite precursor (e.g. Aissaoui, 1985; Savard *et al.* 1996), a carbonate

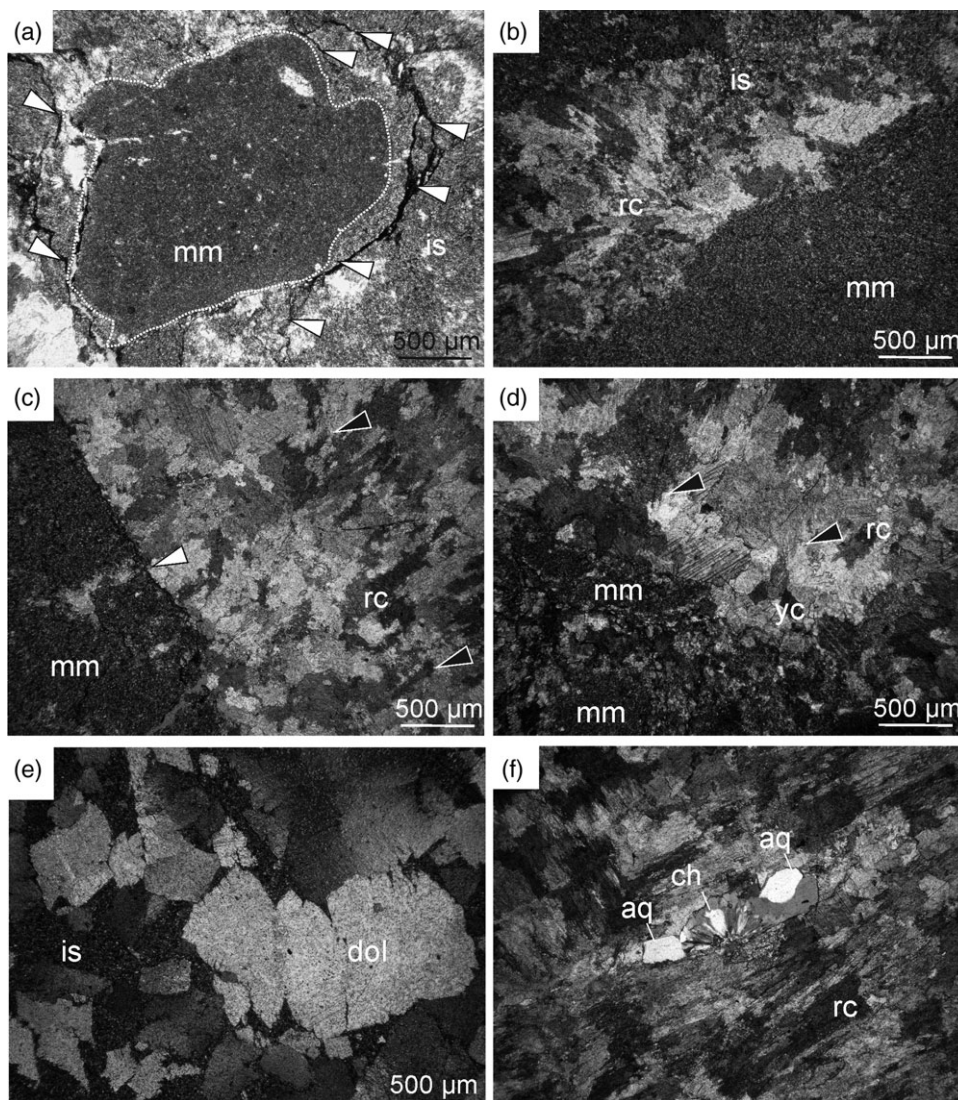


**Fig. 11.** Stromatolitic facies of the Tanohama limestone. (a) Thin-section photomicrograph showing nodule of micritic matrix (mm) floating in internal sediment (is); pressure-solution seams (white arrows) encircle the nodule and affect the internal sediment surrounding it, but do not distort the nodule's margin (white stippled line). Cross-polarized light image. (b) Thin-section photomicrograph showing a fragment of a large micritic nodule (mm) floating in internal sediment (is), with the remaining space occluded by radiaxial cement (rc). Cross-polarized light image. (c) Thin-section photomicrograph showing surface of a fractured nodule of micritic matrix (mm) covered with radiaxial cements (rc). The fracturing predates the formation of cement crust as indicated by the cross-cutting relationship (white arrow). Cross-polarized light image. (d) Thin-section photomicrograph showing corroded surface of fractured micritic nodules (mm) covered with yellow calcite (yc), followed by radiaxial cement crust (rc). Cross-polarized light image. (e) Thin-section photograph showing subhedral dolomite (dol) formed in mixed carbonate-siliciclastic internal sediment (is). Cross-polarized light image. (f) Thin-section photograph showing a cavity within a radiaxial cement crust (rc) filled with chalcidony (ch) followed by anhedral quartz (aq). Cross-polarized light image.

mineral dominating many recent seeps (e.g. Feng *et al.* 2008; Zwicker *et al.* 2018). Aragonite cements form preferentially over calcite cements in waters rich in sulphate anions in aragonite seas (e.g. Hardie, 1996; Savard *et al.* 1996; Zwicker *et al.* 2015), implying that the radiaxial cements at Tanohama formed mostly close to the seabed.

Radiaxial fibrous cements at Tanohama are associated with yellow cements (Figs 10d and 11d). An association of yellow and radiaxial cements is typical of ancient seep carbonates (e.g. Beauchamp & Savard, 1992; Campbell *et al.* 2002; Peckmann *et al.* 2002; Himmler *et al.* 2008; Hammer *et al.* 2011; Hryniewicz *et al.* 2016; Zwicker *et al.* 2018). The yellow cements in ancient seep carbonates are among the most  $^{13}\text{C}$ -depleted carbonate phases present (e.g. Kuechler *et al.* 2012; Zwicker *et al.* 2015) and contain a major portion of molecular fossils typical of AOM-mediating microbial consortia, indicating formation in direct proximity to the loci of AOM (Hagemann *et al.* 2013). The yellow calcites are indeed among the most  $^{13}\text{C}$ -depleted carbonate phases at Tanohama ( $\delta^{13}\text{C}$  values from  $-41.0$  ‰ to  $-32.3$  ‰). In the absence of AOM-specific molecular fossils, the association of  $^{13}\text{C}$  depleted yellow and radiaxial cements at Tanohama is another evidence for seep-related origin of this carbonate deposit.

Cement-filled cavities at Tanohama are occasionally lined with clotted carbonate, underlying other cement phases (Fig. 10c). Individual clots in the Tanohama limestone are small (up to  $100\ \mu\text{m}$  across), rounded to oval structures with irregular boundaries. Much larger structures ( $1\text{--}2\ \text{mm}$  across) with sharp boundaries and occasionally internal structuring have been broadly interpreted as faecal pellets (e.g. Peckmann *et al.* 2002; Peckmann *et al.* 2007; Senowbari-Daryan *et al.* 2007). The latter usually appear in large numbers in different facies within the same seep deposit, and are taken as an indicator that carbonate formation has taken place mostly within the sediment (Hryniewicz *et al.* 2012). The small size, irregular boundaries and localized occurrence of the clots from Tanohama inside some cement-filled cavities indicate that they do not have a faecal origin, and are instead locally precipitated. Similar clotted fabrics have been reported from different seep deposits on a number of occasions (e.g. Peckmann *et al.* 1999, 2011, 2013; Kiel & Peckmann, 2008; Kuechler *et al.* 2012; Agirrezabala *et al.* 2013; Hryniewicz *et al.* 2015), and have been interpreted to be a result of microbially mediated carbonate precipitation (Peckmann *et al.* 2002; Feng *et al.* 2008). Although clotted microfabrics are not exclusive to seeps and occur in other carbonate environments (cf. Flügel, 2004), their localized occurrence close to the  $^{13}\text{C}$ -depleted

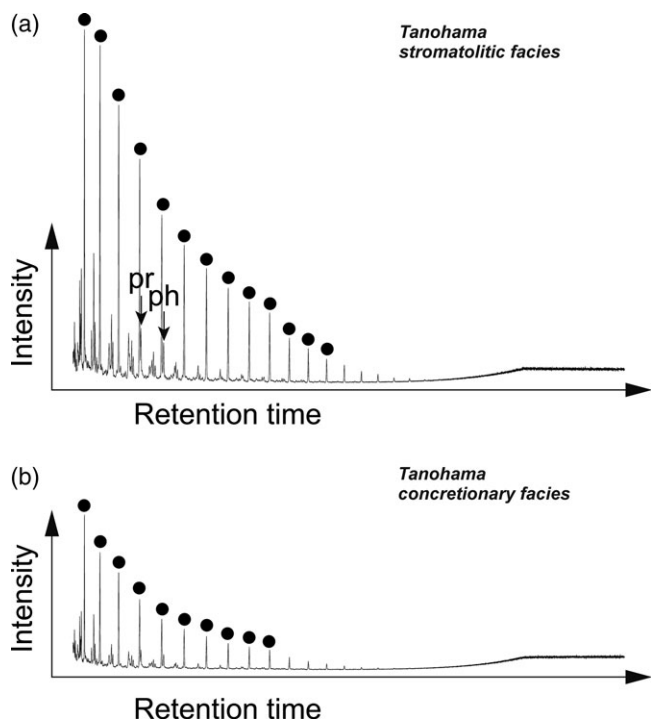


**Fig. 12.** Total ion chromatogram of the hydrocarbon fraction obtained from the Tanohama limestone from (a) stromatolitic facies and (b) concretionary facies. Closed circles indicate *n*-alkanes, and numbers above them indicate the number of carbon atoms. UCM – unresolved complex mixture. Pr – pristane; ph – phytane.

cements at Tanohama indicates they were likely influenced by microbially mediated AOM.

Both Kanoura and Tanohama exhibit nodular fabrics, especially well developed at Tanohama where laminated nodules occur encased in the stromatolitic crust (Fig. 9e). Their  $\delta^{13}\text{C}$ -depleted signatures ( $-23.4\text{‰}$  to  $-22.9\text{‰}$ ) indicate that they incorporated methane-derived carbon, although other sources likely contributed to the less negative  $\delta^{13}\text{C}$  values of the nodule's carbonate compared to the cement phases. This implies that the nodules formed at some distance from centres of AOM at Tanohama, either in the lateral zone of the seep where seepage was somewhat less intense, or deeper in the sediment. Indeed, recent carbonate nodules usually form at seeps at depth in the sediment column and are tied to lower methane concentrations (Haas *et al.* 2010). Laminated fabrics and changing  $\delta^{13}\text{C}$  values of particular laminae can be interpreted as results of fluctuating seepage conditions (e.g. Feng *et al.* 2010), although they can also reflect the presence of microbial mats on the surface of the nodules (e.g. Reitner *et al.* 2005). Some evidence for fluctuating seepage intensities may come from the presence of quartz and chalcedony within cavities (Fig. 11f). Mobilization of silica at seeps is possible during stages of intense fluid flow, when bubble formation and  $\text{CO}_2$  degassing results in rise of alkalinity, while waning fluid flow favours silica reprecipitation (Kuechler *et al.* 2012; Smrzka *et al.* 2015). Nonetheless, moderately low  $\delta^{13}\text{C}$  signatures ( $-23.4\text{‰}$  to  $-22.9\text{‰}$ ) of nodules are somewhat comparable with the values of micrites from the same site ( $-26.5\text{‰}$  to  $-15.3\text{‰}$ ), indicating formation from a mixed carbon pool within the sediment. Lastly, low  $\delta^{13}\text{C}$  signatures of one of the bivalve shells from Tanohama ( $-32.4\text{‰}$ ) can be explained by sample contamination with  $\delta^{13}\text{C}$ -depleted carbonate phases, such as yellow calcites or radial fibrous cements. The other bivalve shell sample from this site that was analysed ( $-4.7\text{‰}$ ) is closer to the

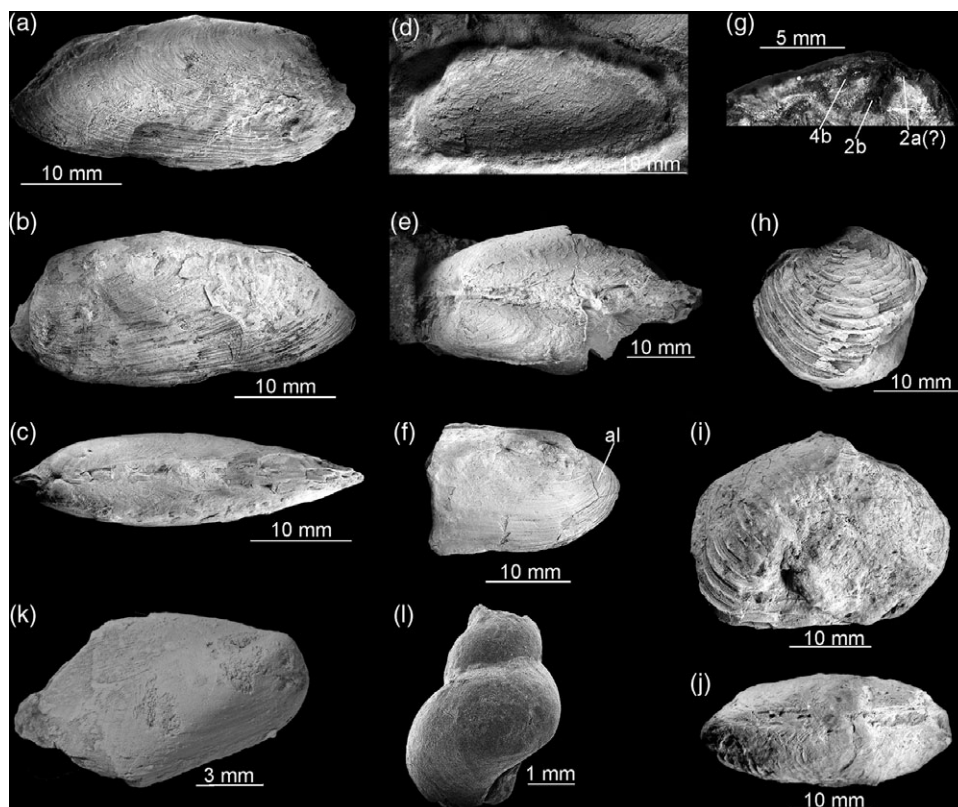


**Fig. 13.** Fossils from Tanohama limestone. (a–g) Vesicomimid bivalve *Pleurophopsis* cf. *hamuroi* (Amano & Kiel, 2011); (a–c) Right- (a) and left- (b) lateral, and dorsal (c) views of a complete specimen. Shell. ZPAL V.55/10. (d) Left-lateral view. Shell. ZPAL V.55/11. (e) Dorsal view of a butterflyed specimen. Partial shell. ZPAL V.55/12. (f) Right-lateral view showing the anterior lobe (al). Partial shell. ZPAL V.55/13. (g). Details of the cardinal dentation of the left valve. Shell. ZPAL V.55/14. (h–j) *Lucinoma* sp. (h) Left-lateral view. Partial shell. ZPAL V.55/15. (i–j) Right-lateral (i) and dorsal (j) views. Shell. ZPAL V.55/16. (k) ‘*Bathymodiolus*’ *akanudaensis* (Kuroda, 1931). Partial shell. GKZ-N00002. (l) *Provanna*? sp. GKZ-N00003.

values normally expected from the shells of chemosymbiotic bivalves (Rio *et al.* 1992; Walliser *et al.* 2019), although it was also likely contaminated by lighter carbonate phases.

### 5.b. Diagenesis of the Taishu Group

At least four lines of evidence indicate that the authigenic carbonates from the Taishu Group have been influenced by diagenetic alterations. These are (i) CL response of cements; (ii) the  $\delta^{18}\text{O}$  values of calcites; (iii) ankerite and its  $\delta^{13}\text{C}$  and  $\delta^{18}\text{O}$  signatures; (iv) the preservation of molecular fossils.

The earliest stage of diagenesis of carbonates at all three sites is revealed by CL imaging, which shows variable degrees of luminescence (Figs 4b, 7d and 10f). Luminescence in carbonates is caused by the presence of the  $\text{Mn}^{2+}$  activator, which under reducing conditions is incorporated into the structure of carbonates, giving them orange luminescence. After the manganese is expended, reduction of  $\text{Fe}^{3+}$  to  $\text{Fe}^{2+}$  and incorporation of the latter progressively quenches carbonate luminescence (Machel *et al.* 1991; Boggs & Krinsley, 2006). Likewise, orange and dull luminescence of recrystallized matrix of the Fukuzaki limestone implies it has recrystallized in contact with reducing pore fluids. Notably, radial cements from Kanoura show small non-luminescent enclaves floating within a luminescent crust (Fig. 7d). In general, luminescence responses of radial cements vary depending on local redox conditions, and both orange- (e.g. Little *et al.* 2015) and blue- (e.g. Hammer *et al.* 2011) luminescent cements have been documented. Yet, it is apparent that radial cements from Kanoura express peripheral recrystallization under the influence of diagenetic fluids. Limited influence of diagenetic fluids on radial cements at Tanohama is, on the other hand, revealed by their low luminescence (Fig. 10f).

The  $\delta^{18}\text{O}$  signatures of calcites from the Fukuzaki and Kanoura limestones are very negative, and cluster between  $-14.4\text{‰}$  and  $-10.4\text{‰}$ . Such low values differ greatly from near-zero or positive  $\delta^{18}\text{O}$  values of calcites and aragonite commonly observed at modern seeps (e.g. Feng *et al.* 2008; Haas *et al.* 2010; Himmeler *et al.* 2015). In many cases, seep cements show  $\delta^{18}\text{O}$  signatures similar to that of local bottom waters. Factors like gas hydrate destabilization and clay mineral dehydration in the subsurface can contribute to the overall oxygen isotope budget of interstitial fluids to some extent, and alter the principal seawater signature (e.g. Bohrmann *et al.* 1998; Greinert *et al.* 2002; Dählmann & De Lange, 2003; Mazzini *et al.* 2005; Feng *et al.* 2014). Both factors, however, cause seeping fluids to be more  $^{18}\text{O}$ -enriched, which translates into higher  $\delta^{18}\text{O}$  signatures of precipitating seep cements. This is not the case for the Taishu Group. Instead, the very low  $\delta^{18}\text{O}$  signatures indicate fluids either with low  $\delta^{18}\text{O}$  values, or an increased temperature. Possible causes could be influx of meteoric waters, burial diagenesis or precipitation from hydrothermal fluids. Major meteoric water influx seems unlikely for relatively deep-water sediments of the Taishu Group (Ninomiya *et al.* 2020). However, marginal marine and deltaic environments have been identified in some sections of the unit (Nakajo, 1998; Nakajo & Maejima, 1998). Given that freshwater can penetrate sedimentary successions even far from land (cf. Kooi & Groene, 2001), and that marginal marine deposits developed southwards of the present-day outcrops of the Taishu Group, periodic freshwater influx cannot be excluded, at least for the southernmost site (Fukuzaki).

The presence of ankerite at Kanoura (Fig. 7; Table 1), on the other hand, can be related to the burial diagenesis. In sedimentary environments, ankerite forms from fluids containing reduced iron and, at the same time, no free sulphide which would otherwise bind

the iron (e.g. Pye *et al.* 1990). That indicates formation from sulphide-poor waters below the bacterial sulphate reduction zone. Assuming that burial fluids within the Taishu Group were largely marine, and that they maintained a near-equilibrium with the coeval seawater (Krajewski *et al.* 2001), the  $\delta^{18}\text{O}$  values of the ankerite microspar ( $-11.1\text{‰}$  to  $-9.7\text{‰}$  VPDB) translate to precipitation temperatures of *c.* 50 to 110 °C (Fisher & Land, 1986). The  $\delta^{13}\text{C}$  values of the ankerite microspar, spanning from  $-19.5\text{‰}$  to  $-7.1\text{‰}$ , indicate precipitation from a mixture of inorganic and organic sources, likely coming from dissolution of detrital and skeletal carbonate and thermal decarboxylation of organic matter (Krajewski & Woźny, 2009).

Remarkably, the radial cements from the Tanohama limestone exhibit much higher  $\delta^{18}\text{O}$  values ( $-5.0\text{‰}$  to  $-2.4\text{‰}$  VPDB), at odds with  $\delta^{18}\text{O}$  signatures of the remaining carbonate phases from this deposit. The yellow cements, micrites and micritic nodules are strongly  $^{18}\text{O}$ -depleted ( $-13.8\text{‰}$  to  $-12.4\text{‰}$  VPDB) and thus more comparable with respect to analogous phases from Fukuzaki and Kanoura limestones (Figs 3 and 6; Table 1). The pattern observed indicates that burial fluids had an influence on the Tanohama seep deposit, but their effect on radial cements was less than for the Kanoura deposit. This is likely because radial cements at Tanohama are particularly thick, and the low porosity typical of this fabric (Aïssaoui, 1985) has prevented burial fluids from influencing their  $\delta^{18}\text{O}$  signatures to a degree comparable to that observed at Kanoura.

Further heating beyond the temperatures recorded by the cements is suggested by the preservation state of the enclosed organic matter. Normal-alkanes (*n*-alkanes) are chief hydrocarbon compounds preserved in all of the investigated seep carbonates, and isoprenoid biomarkers of methane-oxidizing archaea (ANME), such as pentamethylcosane (PMI) and crocetane, were not detected (Fig. 12). Alkanes preserved in the Fukuzaki and Kanoura limestones range from *n*-C<sub>17</sub> to *n*-C<sub>31</sub>, with bimodal distribution maximizing at *n*-C<sub>18</sub> and around *n*-C<sub>26</sub> and *n*-C<sub>27</sub> alkanes. *n*-Alkanes with high carbon numbers (23 to 31) are partially in the range of those normally expected for the leaf waxes or freshwater algae (e.g. Eglinton & Hamilton, 1967; Gelpi *et al.* 1970). However, no odd-to-even predominance at Fukuzaki and Kanoura suggests that the observed carbon number pattern of alkanes is not source-related. Marine algae produce short-chain *n*-alkanes (*n*-C<sub>15</sub> to *n*-C<sub>19</sub>) with odd-to-even predominance, also unlike the samples from the current materials. The presence of an unresolved complex mixture in seep carbonates is usually interpreted as an input from biodegraded oil (e.g. Naehr *et al.* 2009). However, the carbonates studied have very low contents of total organic carbon (TOC; < 0.1%), which would be larger if oil was indeed incorporated. Therefore, the pattern of *n*-alkanes observed at Fukuzaki and Kanoura limestones is best explained as a result of thermal cracking of organic matter, with some input from terrigenous higher plants and non-marine/marine algae. The unimodal distribution of *n*-alkanes with short-chain predominance at Tanohama could be obviously ascribed to thermal maturity of the enclosed organic matter (Peters *et al.* 2005). It is thus highly possible that the biomarkers of ANME have been degraded due to thermal cracking within the seep carbonates. The strongly  $^{13}\text{C}$ -depleted signatures of TOC of the studied carbonates ( $-36\text{‰}$ ,  $-42\text{‰}$  and  $-49\text{‰}$  at Kanoura, Fukuzaki and Tanohama, respectively) imply that the seep carbonates contain some amounts of AOM-related organic compounds. Therefore, the observed *n*-alkanes might in some part originate from thermal cracking of ANME lipids. A possible heat source could be increased

burial during middle Miocene folding (Golozubov *et al.* 2017) and associated intrusive activity (Miti, 1972, 1973, 1974).

### 5.c. Chemosynthesis-based palaeoecosystems of the Taishu Group

The fauna of the cold seep carbonates from the Taishu Group comprises two species of the vesicomyid bivalve *Pleurophopsis*, a species of the bathymodiolin bivalve '*Bathymodiolus*', a species of the lucinid bivalve *Lucinoma*, a gastropod possibly belonging to *Provanna*, and agglutinated worm tubes (Figs 3, 5, 8 and 13). Vesicomyid and bathymodiolin bivalves are obligate members of seep communities since the Eocene (Amano and Kiel, 2007; Kiel & Amano, 2013; see Kiel, 2010 and references therein for discussion of obligate seep fauna), and have no confirmed pre-Eocene fossil record. Such a fossil record is congruent with the hypothesis that evolutionary radiations of both groups started in the Eocene, and is related to the acquisition of symbiosis with sulphide-oxidizing bacteria (Lorion *et al.* 2013; Johnson *et al.* 2017), with some bathymodiolins acquiring methanotrophic symbioses during subsequent radiations in the Miocene. The vesicomyid *Pleurophopsis* is one of the most common and species-rich vesicomyids in Eocene–Miocene seep faunas of the Northern Pacific (Amano and Kiel, 2007, 2011; Kiel, 2007; Amano *et al.* 2019a; Kiel *et al.* 2019, 2020), and its presence in the lower Miocene Taishu Group is concordant with its known palaeogeographic and stratigraphic range. Likewise, the fossil '*Bathymodiolus*' is a member of Eocene and younger fossil seep faunas worldwide (e.g. Saether *et al.* 2010b; Amano & Jenkins, 2011b; Kiel & Amano, 2013; Kiel & Taviani, 2017), and thus its presence in the early Miocene seep fauna from the Taishu Group is also concordant with the stratigraphic range of this genus. Among them, it has been elucidated that '*Bathymodiolus*' *akanudaensis* is an endemic species of the early to middle Miocene Sea of Japan, corresponding to the oldest record of the species.

In contrast to vesicomyid clams and bathymodiolin mussels, *Lucinoma* and a possible *Provanna* from the Taishu Group seep deposits have been previously unknown. However, taking into account the frequent occurrence of *Lucinoma* at Neogene seeps from Japan (Majima *et al.* 2005; Amano *et al.* 2010; Miyajima *et al.* 2018), and its relatively high frequency at Cenozoic and especially Miocene seeps worldwide (e.g. Kiel & Taviani, 2017, 2018; Amano *et al.* 2018; Kiel *et al.* 2020), its presence at the Miocene seeps of the Taishu Group is in agreement with the palaeogeographic setting and age of these seep deposits. Cenozoic provannids, especially *Provanna*, are widespread in Eocene–Miocene seeps and cognate communities from the circum-Pacific area (e.g. Squires, 1995; Saether *et al.* 2010a; Amano & Jenkins, 2013; Amano & Little, 2014; Hybertsen & Kiel, 2018; Kiel *et al.* 2020). Consequently, a possible *Provanna* from the Miocene seeps of the Taishu Group fits well into the palaeogeographic and stratigraphic context of the deposit. Moreover, *Lucinoma* and a putative *Provanna* are also the oldest fossil records of each taxa from the Sea of Japan side.

Overall, the molluscan fauna discussed here has a classical Cenozoic character, especially well expressed at Oligocene–Miocene deep-water seeps of the northern circum-Pacific area (e.g. Amano *et al.* 2019a; Kiel *et al.* 2020), and includes at least the four oldest records of the species on the Sea of Japan side.

Annelids which construct agglutinated tubes and occur at seeps belong to the families Maldanidae, Terebellidae, Ampharetidae and Sabellidae (Levin *et al.* 2003; Turnipseed *et al.* 2004; Levin & Mendoza, 2007). These are generally not considered to be seep-obligate as they do not obtain their nutrition directly from

chemosynthetic microbial symbionts, and often also occur in nearby non-seep environments. However, recently it was surprisingly discovered that sabellids can also harbour chemosynthetic symbioses at seeps (Goffredi *et al.* 2020), providing the first instance of this for an annelid that dwells within an agglutinated tube. The prevalence of these symbioses in both modern and fossil seeps is still unknown; it is therefore possible that the Fukuzaki tubes (Fig. 3d) were built by annelid-bearing chemosynthetic symbionts, or that they occupied these seeps to benefit from the increased amounts of organic matter at the site.

## 6. Discussion

### 6.a. Formation of the Sea of Japan and hydrocarbon seepage

The existing hypothesis about the formation of the Sea of Japan involves either a rather prolonged process lasting from the Palaeogene to middle Miocene (e.g. Lallemand & Jolivet, 1985; Nakada *et al.* 1997), or a sudden event in the early and middle Miocene (e.g. Ingle, 1992; Jolivet & Tamaki, 1992; Ninomiya *et al.* 2014, 2017). The purpose of our study is not to resolve which of the two models is correct, but rather to place the hydrocarbon seepage recorded in the Taishu Group in a geological context. An important point for further discussion is also that the early Miocene hydrocarbon seeps from the Taishu Group belong to the oldest known hydrocarbon seep carbonates from the Sea of Japan (e.g. Amano *et al.* 2019a). Consequently, they record the earliest examples of hydrocarbon generation and expulsion in this basin.

Several fossil seep carbonates have been reported from ancient marine deposits bordering the eastern part of the Sea of Japan (e.g. Majima *et al.* 2005; Amano *et al.* 2010; Miyajima *et al.* 2016, 2017, 2018). The great majority of these deposits, for example, the middle Miocene carbonates from the Bessho Formation in Nagano Prefecture, with  $\delta^{13}\text{C}$  signatures around  $-40\text{‰}$  or heavier (e.g. Miyajima *et al.* 2017, 2018), the uppermost middle Miocene Kita-Kuroiwa seep deposit from Ogaya Formation, Niigata Prefecture, with  $\delta^{13}\text{C}$  signatures as low as  $-36.0\text{‰}$  (e.g. Amano *et al.* 2010) and the upper Miocene Nakanomata seep deposit from the Nodani Formation, Niigata Prefecture, with  $\delta^{13}\text{C}$  values as low as  $-41.1\text{‰}$  (Miyajima *et al.* 2016), document seepage of methane of biogenic or mixed biogenic/thermogenic origin. The geotectonic setting of the Sea of Japan seems favourable for generation, accumulation and release of the methane-rich fluids. Extensional tectonics which were active during the early Miocene in the eastern Sea of Japan have been replaced by compressional tectonics from the late Miocene – middle Pliocene onwards (e.g. Jolivet & Tamaki, 1992; Okui *et al.* 2008). Both extensional and compressional tectonic regimes are favourable for submarine hydrocarbon seepage. For example, extensional tectonics favour accumulation of thick sedimentary successions and hydrocarbon migration along normal faults (e.g. Sibuet & Olu, 1998), and compressional tectonics enhance trapping of hydrocarbons and their subsequent escape from anticlinal structures (e.g. Okui *et al.* 2008; Ding *et al.* 2010). The link between compressional tectonics and seepage has so far been especially well documented in the Sea of Japan, as several late Miocene and Pliocene seep carbonates from the eastern part of the sea are located close to the axes of anticlinal structures (Amano & Kanno, 2005; Amano & Jenkins, 2011a; Miyajima *et al.* 2018), a pattern which is also observed for the extant seeps in this area (e.g. Okui *et al.* 2008).



In contrast to the well-documented late Miocene – Recent cold seeps and their relationship with compressional tectonics, seep deposits from Tsushima described in this paper record an initial period of hydrocarbon seepage in the Sea of Japan, when compressional tectonics were still inactive. The deposition of the Taishu Group was a rather rapid event, taking place roughly between 17.9 and 15.9 Ma, close to the end of the early Miocene (Ninomiya *et al.* 2014). It involved development of a pull-apart basin and its rapid filling with up to 5400 m of siliciclastic deposits, which gives an averaged sedimentation rate of up to 2.7 m per 1000 years (Golozubov *et al.* 2017). However, because the rocks exposed today are compacted, the initial thickness of the succession and thus the actual sedimentation rate was likely higher. This is a high depositional rate when compared with those from typical deep water environments where extant seeps are usually encountered (e.g. Cita *et al.* 1978; Wefer *et al.* 1998; Smith *et al.* 2014), but comparable with high depositional rates from sediment mass-wasting areas. Implications of these are (i) the thick sedimentary package of the Taishu Group trapped large volumes of fluids, and (ii) organic matter trapped in the sediment was deeply and rapidly buried. Pore fluids trapped during rapid deposition of sediments are susceptible to migration and expulsion when over-pressured, which initiates subsurface fluid flow (Judd & Hovland, 2007). As the Taishu Group was deposited in a rapidly down-warped basin which experienced syndimentary landslide faulting (Golozubov *et al.* 2017; Ninomiya *et al.* 2020), possible fluid migration pathways include various shallow to deep-rooted faults. We do not expect that the folding and intrusive activity was a major factor influencing fluid migration, since it was a post-depositional event, dated as *c.* 15 Ma (Golozubov *et al.* 2017). Extant geological equivalents of early Miocene seeps from the Taishu Group could comprise, for example, cold seeps along the Marmara Fault in the Sea of Marmara, Turkey, where strike-slip tectonics cause pull-apart basin formation and submarine fluid seepage in relative proximity (e.g. Zitter *et al.* 2008; Ritt *et al.* 2010).

### 6.b. Miocene chemosynthesis-based faunas of the Sea of Japan

Miocene seep faunas from Japan are characterized by frequent occurrence of the vesicomid bivalve *Pleurophopsis*, found in addition to ‘*Bathymodiolus*’ mussels, the gastropod *Provanna*, the lucinid *Lucinoma* and others (Amano *et al.* 2019a and references therein). *Pleurophopsis* is known from the late Eocene – late Miocene of the eastern Pacific (Amano and Kiel, 2007; Kiel, 2007; Kiel & Hansen, 2015; Kiel *et al.* 2020). The fossil record of *Pleurophopsis* in Japan, on the other hand, is somewhat narrower, and spans from the late Oligocene – early Miocene to the Pliocene (Amano *et al.* 2019a). The acme of *Pleurophopsis* in Japan coincides with the early–middle Miocene interval, when at least six species occurred at seeps of the Sea of Japan, four of them endemic to it (Amano *et al.* 2019a). This is more than on the Pacific side of Japan, where up to four species have been reported so far (Amano *et al.* 2019a). In addition to its frequent occurrence at seeps from that time, *Pleurophopsis* is also found in ‘normal’, deep-water deposits of Japan, where it was apparently redeposited (Amano *et al.* 2014, 2019b), which underlines its ubiquity and broad distribution in regional deep-water benthic environments at that time.

While the late Miocene decline of *Pleurophopsis* in Japan has been linked with cooling that occurred at that time, as evidenced by establishment of cold-water *Calyptogenia pacifica* Dall, 1891 in the late Miocene (e.g. Amano & Jenkins, 2011a; Amano *et al.*

2019a), the reasons for the early–middle Miocene proliferation of *Pleurophopsis* in Japan remain elusive. Given that it roughly coincides with the warm climatic period culminating in the so-called Mid-Neogene Climatic Optimum around the early/late Miocene transition (Tsuchi, 1990), a climatic reason could be responsible. At least in the case of other Miocene chemosymbiotic bivalves, *Acharax yokosukensis* Kanie & Kuramochi, 1995 (Amano & Ando, 2011) and the lucinid *Epilucina californica* (Conrad, 1837), the warm climate seemed to have influenced their Miocene history, allowing *A. yokosukensis* to grow to unusually large sizes (Amano & Ando, 2011), and facilitating *E. californica* dispersal from North America to Japan (Kurihara, 2007). Higher temperatures might be beneficial for chemosymbiotic bivalves which are able to withstand them, mostly because of faster bivalve growth, enhanced symbiont metabolism and resulting higher rates of carbon fixation (Girguis & Childress, 2006; Childress & Girguis, 2011), as long as the increased oxygen demands of bacterial–bivalve symbiosis are met.

## 7. Conclusions

This study documents evidence of ancient hydrocarbon seepage and oxidation, preserved within authigenic carbonates from the lower Miocene Taishu Group from Tsushima, Japan. The investigation included deposits from Fukuzaki, Kanoura and Tanohama limestones, i.e. three out of the four initially reported by Ninomiya (2011). The observed textures, such as radial and yellow cements, and clotted micrites, together with notable <sup>13</sup>C depletion of the carbonates indicate their formation due to oxidation of methane of biogenic or mixed biogenic/thermogenic origin. The fauna of these carbonates comprises two species of vesicomid bivalve *Pleurophopsis*, a species of the bathymodiolid mussel ‘*Bathymodiolus*’, a species of lucinid bivalve *Lucinoma*, a possible provannid gastropod (*Provanna?*), which is common in Miocene seep carbonates from the ancient Sea of Japan, and agglutinated worm tubes. All of the investigated carbonates formed in a rapidly subsiding pull-apart basin *c.* 17.9–15.9 Ma, during an initial stage of opening of the Sea of Japan, and are among the oldest seep carbonates from this area. The authigenic carbonates from Tsushima formed before a major compressive event, while their younger equivalents from other parts of the Sea of Japan (Honshu) are often associated with compressive features, such as anticlines.

**Acknowledgements.** This work was performed in part in the NanoFun laboratory co-financed by the European Regional Development Fund within the Innovation Economy Operational Programme POIG.02.02.00-00-025/09. We would like to thank Przemysław Gorzelak for assistance during CL photography, and Ewa Durska (both Warsaw) for acid dissolution of carbonates and analysis of organic residues. Akihiro Kano (The University of Tokyo) generously performed carbon and oxygen isotope analysis. We gratefully acknowledge Soichiro Muta, Akiko S. Goto and Takashi Hasegawa (Kanazawa University) for support in biomarker and TOC analyses, as well as carbon and oxygen isotope measurements. Funding for KH was provided by the National Science Centre (NCN), Poland, research grant no. 2014/15/B/ST10/04886 entitled ‘The influence of Paleocene/Eocene Thermal Maximum on oceanic chemosynthesis-based ecosystems’. This study was also financially supported by Grant-in-Aid (KAKENHI) from the Japan Society for the Promotion of Science (JSPS) for JSPS Research Fellow to YM (No. 15J01158). MJ was supported by the National Science Centre, Poland, grant no. 2016/23/D/ST10/00444. MG is grateful for support from the United Kingdom Natural Environment Research Council (NERC), grant number NE/R000670/1. Special thanks go to Steffen Kiel and an anonymous reviewer whose comments helped significantly to improve the manuscript.

**Supplementary material.** To view supplementary material for this article, please visit <https://doi.org/10.1017/S001675682000103X>

## References

- Agirrezabala LM, Kiel S, Blumenberg M, Schäfer N and Reitner J** (2013) Outcrop analogues of pockmarks and associated methane-seep carbonates: a case study from the Lower Cretaceous (Albian) of the Basque-Cantabrian Basin, western Pyrenees. *Palaeogeography, Palaeoclimatology Palaeoecology* **390**, 94–115.
- Aïssaoui DM** (1985) Botryoidal aragonite and its diagenesis. *Sedimentology* **32**, 345–61.
- Amano K and Ando H** (2011) Giant fossil *Acharax* (Bivalvia: Solemyidae) from the Miocene of Japan. *The Nautilus* **125**, 207–12.
- Amano K and Jenkins RG** (2011a) Fossil record of extant vesicomid species from Japan. *Venus* **69**, 163–76.
- Amano K and Jenkins RG** (2011b) New fossil *Bathymodiolus* (sensu lato) (Bivalvia: Mytilidae) from Oligocene seep-carbonates in eastern Hokkaido, Japan, with remarks on the evolution of the genus. *The Nautilus* **125**, 29–35.
- Amano K and Jenkins RG** (2013) A new species of *Provanna* (Gastropoda: Provannidae) from an Oligocene seep deposit in Eastern Hokkaido, Japan. *Paleontological Research* **17**, 325–9.
- Amano K, Jenkins RG, Aikawa M and Nobuhara T** (2010) A Miocene chemosynthetic community from the Ogaya Formation in Joetsu: evidence for depth-related ecologic control among fossil seep communities in the Japan Sea back-arc basin. *Palaeogeography, Palaeoclimatology, Palaeoecology* **286**, 184–90.
- Amano K, Jenkins RG, Ohara M and Kiel S** (2014) Miocene vesicomid species (Bivalvia) from Wakayama in southern Honshu, Japan. *The Nautilus* **128**, 9–17.
- Amano K, Jenkins RG, Sako Y, Ohara M and Kiel S** (2013) A Paleogene deep-sea methane-seep community from Honshu, Japan. *Palaeogeography, Palaeoclimatology, Palaeoecology* **387**, 126–33.
- Amano K and Kanno S** (2005) *Calyptogena* (Bivalvia: Vesicomidae) from Neogene strata in the Joetsu district, Niigata Prefecture, central Japan. *The Veliger* **47**, 202–12.
- Amano K and Kiel S** (2007) Fossil vesicomid bivalves from North Pacific region. *The Veliger* **49**, 270–93.
- Amano K and Kiel S** (2011) Fossil *Adulomya* (Vesicomidae, Bivalvia) from Japan. *The Veliger* **51**, 76–90.
- Amano K and Little CTS** (2014) Miocene abyssochrysid gastropod *Provanna* from Japanese seep and whale-fall sites. *Acta Palaeontologica Polonica* **59**, 163–72.
- Amano K, Little CTS and Campbell KA** (2018) Lucinid bivalves from Miocene hydrocarbon seep sites from eastern North Island, New Zealand, with comments on Miocene New Zealand seep faunas. *Acta Palaeontologica Polonica* **63**, 371–82.
- Amano K, Miyajima Y, Jenkins RG and Kiel S** (2019a) The Miocene to Recent biogeographic history of vesicomid bivalves in Japan, with two new records of the family. *The Nautilus* **133**, 48–56.
- Amano K, Miyajima Y, Nakagawa K, Hamuro M and Hamuro T** (2019b) Chemosymbiotic bivalves from the lower Miocene Kurosedani Formation in Toyama Prefecture, central Honshu, Japan. *Paleontological Research* **23**, 208–19.
- Beauchamp B and Savard M** (1992) Cretaceous chemosynthetic carbonate mounds in the Canadian Arctic. *Palaios* **7**, 434–50.
- Boetius A, Ravensschlag K, Schubert CJ, Rickert D, Widdel F, Gieseke A, Amann R, Jørgensen BB, Witte U and Pfannkuche O** (2000) A microbial consortium apparently mediating anaerobic oxidation of methane. *Nature* **407**, 623–6.
- Boggs S and Kinsley D** (2006) *Application of Cathodoluminescence Imaging to the Study of Sedimentary Rocks*. Cambridge: Cambridge University Press, 176 pp.
- Bohrmann G, Greinert J, Suess E and Torres M** (1998) Authigenic carbonates from Cascadia subduction zone and their relation to gas hydrate stability. *Geology* **26**, 647–50.
- Campbell KA** (2006) Hydrocarbon seep and hydrothermal vent paleoenvironments and paleontology: past developments and future research directions. *Palaeogeography, Palaeoclimatology, Palaeoecology* **232**, 362–407.
- Campbell KA, Farmer JD and Des Marais D** (2002) Ancient hydrocarbon seeps from the Mesozoic convergent margin of California: carbonate geochemistry, fluid and palaeoenvironments. *Geofluids* **2**, 63–94.
- Childress JJ and Girguis PR** (2011) The metabolic demands of endosymbiotic chemoautotrophic metabolism on host physiological capacities. *Journal of Experimental Biology* **214**, 312–25.
- Cita MB, Ryan WBF and Kidd RB** (1978) Sedimentation rates in Neogene deep-sea sediments from the Mediterranean and geodynamic implications for their changes. *Initial Reports of the Deep Sea Drilling Project* **42**, 991–1002.
- Conrad TA** (1837) Descriptions of new marine shells from upper California, collected by Thomas Nuttall, Esq. *Journal of the Academy of Natural Sciences of Philadelphia* **7**, 227–68.
- Cosel RV and Janssen R** (2008) Bathymodioline mussels of the *Bathymodiolus* (s.l.) *childressi* from methane seeps near Edison Seamount, New Ireland, Papua New Guinea: (Bivalvia: Mytilidae). *Archiv für Molluskenkunde* **137**, 195–224.
- Dähmann A and De Lange GJ** (2003) Fluid–sediment interactions at Eastern Mediterranean mud volcanoes: a stable isotope study of ODP Leg 160. *Earth and Planetary Science Letters* **212**, 377–91.
- Dall WH** (1891) Scientific results of explorations by the US Fish Commission Steamer *Albatross*. XX. On some new or interesting West American shells obtained from dredgings of the US Fish Commission steamer *Albatross* in 1888. *Proceedings of the US National Museum* **14**, 174–91.
- Dall WH** (1901) Synopsis of the Lucinacea and of the American species. *Proceedings of the United States National Museum* **23**, 779–833.
- Dall WH** (1918) Descriptions of new species of shells, chiefly from Magdalena Bay, Lower California. *Proceedings of the Biological Society of Washington* **31**, 5–8.
- Ding F, Spiess V, Fekete N, Murton B, Brüning M and Bohrmann G** (2010) Interaction between accretionary thrust faulting and slope sedimentation at the frontal Makran accretionary prism and its implications for hydrocarbon fluid seepage. *Journal of Geophysical Research* **115**, B08106.
- Dubilier N, Bergin C and Lott C** (2008) Symbiotic diversity in marine animals: the art of harnessing chemosynthesis. *Nature Reviews: Microbiology* **6**, 725–40.
- Eglinton G and Hamilton RJ** (1967) Leaf epicuticular waxes. *Science* **156**, 1322–35.
- Feng D, Birgel D, Peckmann J, Roberts HH, Joye SB, Sassen R, Liu X-L, Hinrichs K-U and Chen D** (2014) Time integrated variation of sources of fluids and seepage dynamics archived in authigenic carbonate from Gulf of Mexico Gas Hydrate Seafloor Observatory. *Chemical Geology* **385**, 129–39.
- Feng D, Chen D, Peckmann J and Bohrmann G** (2010) Authigenic carbonates from methane seeps of the northern Congo fan: microbial formation mechanism. *Marine and Petroleum Geology* **27**, 748–56.
- Feng D, Chen D and Roberts HH** (2008) Sedimentary fabrics in the authigenic carbonates from Bush Hill: implications for seabed fluid flow and its dynamic signature. *Geofluids* **8**, 301–10.
- Fisher RS and Land LS** (1986) Diagenetic history of the Eocene Wilcox sandstones and associated waters, South-Central Texas. *Geochimica et Cosmochimica Acta* **50**, 551–62.
- Flügel E** (2004) *Microfacies of Carbonate Rocks: Analysis, Interpretation and Application*. Berlin: Springer, 976 pp.
- Gelpi E, Schneider H, Mann J and Oro J** (1970) Hydrocarbons of geochemical significance in microscopic algae. *Phytochemistry* **9**, 603–12.
- Georgieva MN, Little CT, Watson JS, Sephton MA, Ball AD and Glover AG** (2019) Identification of fossil worm tubes from Phanerozoic hydrothermal vents and cold seeps. *Journal of Systematic Palaeontology* **17**, 287–329.
- Girguis PR and Childress JJ** (2006) Metabolite uptake, stoichiometry and chemoautotrophic function of the hydrothermal vent tubeworm *Riftia pachyptila*: responses to environmental variations in substrate concentrations and temperature. *Journal of Experimental Biology* **209**, 3516–28.
- Goffredi SK, Tilic E, Mullin SW, Dawson KS, Keller A, Lee R, Wu F, Levin LA, Rouse GW, Cordes E and Orphan VJ** (2020) Sequestration of methane

- by symbiotic deep-sea annelids: ancient and future implications of redefining the seep influence. *Science Advances* **6**, eaay8562.
- Golozubov VV, Kasatkin SA, Yokoyama K, Tsutsumi Y and Kiyokawa S** (2017) Miocene dislocations during the formation of Sea of Japan basin: case study of Tsushima Islands. *Geotectonics* **51**, 412–27.
- Greinert J, Bohrmann G and Elvert M** (2002) Stromatolitic fabric of authigenic carbonate crust: results of anaerobic methane oxidation at cold seeps in 4,850 m water depth. *International Journal of Earth Sciences* **91**, 698–711.
- Haas A, Peckmann J, Elvert M, Sahling H and Bohrmann G** (2010) Patterns of carbonate authigenesis at the Kouilou pockmarks on the Congo deep-sea fan. *Marine Geology* **268**, 129–36.
- Hagemann A, Leefmann T, Peckmann J, Hoffmann V-E and Thiel V** (2013) Biomarkers from individual carbonate phases of an Oligocene cold-seep deposit, Washington State, USA. *Lethaia* **46**, 7–18.
- Hammer Ø, Nakrem HA, Little CTS, Hryniewicz K, Sandy MR, Hurum JH, Druckenmiller P, Knutsen EM and Høyberget M** (2011) Hydrocarbon seeps from close to the Jurassic–Cretaceous boundary. *Palaeogeography, Palaeoclimatology, Palaeoecology* **306**, 15–26.
- Hardie LA** (1996) Secular variation in seawater chemistry: an explanation for the coupled secular variation in the mineralogies of marine limestones and potash evaporites over the past 600 my. *Geology* **24**, 279–83.
- Hikida Y, Suzuki S, Togo Y and Ijiri A** (2003) An exceptionally well-preserved fossil seep community from the Cretaceous Yezo Group in the Nakagawa area, Hokkaido, northern Japan. *Paleontological Research* **7**, 329–42.
- Himmler T, Birgel D, Bayon G, Pape T, Ge L, Bohrmann G and Peckmann J** (2015) Formation of seep carbonates along Makran convergent margin, northern Arabian Sea, and a molecular and isotopic approach to constrain the carbon isotopic composition of parent methane. *Chemical Geology* **415**, 102–17.
- Himmler T, Brinkmann F, Bohrmann G and Peckmann J** (2011) Corrosion patterns of seep carbonates from the eastern Mediterranean Sea. *Terra Nova* **23**, 206–12.
- Himmler T, Freiwald A, Stollhofen H and Peckmann J** (2008) Late Carboniferous hydrocarbon-seep carbonates from the glaciomarine Dwyka Group, southern Namibia. *Palaeogeography, Palaeoclimatology, Palaeoecology* **257**, 185–97.
- Hryniewicz K, Bitner MA, Durska E, Hagström J, Hjalmsrédóttir HR, Jenkins RG, Little CTS, Miyajima Y, Nakrem HA and Kaim A** (2016) Paleocene methane seep and wood-fall marine environments from Spitsbergen, Svalbard. *Palaeogeography, Palaeoclimatology, Palaeoecology* **462**, 41–56.
- Hryniewicz K, Hammer Ø, Nakrem HA and Little CTS** (2012) Microfacies of the Volgian–Ryazanian (Jurassic–Cretaceous) hydrocarbon seep carbonates from Sassenfjorden, central Spitsbergen, Svalbard. *Norwegian Journal of Geology* **92**, 113–31.
- Hryniewicz K, Hagström J, Hammer Ø, Kaim A, Little CTS and Nakrem HA** (2015) Late Jurassic–Early Cretaceous hydrocarbon seep boulders from Novaya Zemlya and their faunas. *Palaeogeography, Palaeoclimatology, Palaeoecology* **436**, 231–44.
- Hybertsen F and Kiel S** (2018) A middle Eocene seep deposit with silicified fauna from the Humpulips Formation in western Washington State, USA. *Acta Palaeontologica Polonica* **63**, 751–68.
- Ingle JC Jr** (1992) Subsidence of the Japan Sea: stratigraphic evidence from ODP sites and onshore sections. *Proceedings of the Ocean Drilling Program, Scientific Results* **127/128**, 1197–1218.
- Isomi H and Nagahama H** (1964) Unconformity between the Taishu Group and the Pliocene Ebishima Formation in the northernmost part of the Tsushima Islands, west Japan – a contribution to the age problem of the Taishu Group. *Journal of the Geological Society of Japan* **71**, 32–5.
- Jakubowicz M, Dopieralska J and Belka Z** (2015) Tracing the composition and origin of fluids at an ancient hydrocarbon seep (Hollard Mound, Middle Devonian, Morocco): A Nd, REE and stable isotope study. *Geochimica et Cosmochimica Acta*, **156**, 50–74.
- Jakubowicz M, Hryniewicz K and Belka Z**, (2017) Mass occurrence of seep-specific bivalves in the oldest-known cold seep metazoan community. *Scientific Reports* **7**, 14292.
- Jenkins RG, Kaim A, Hikida Y and Tanabe K** (2007) Methane-flux-dependent lateral faunal changes in a Late Cretaceous chemosymbiotic assemblage from the Nakagawa area of Hokkaido, Japan. *Geobiology* **5**, 127–39.
- Johnson SB, Krylova EM, Audzijonyte A, Sahling H and Vrijenhoek RC** (2017) Phylogeny and origins of chemosynthetic vesicomid clams. *Systematics and Biodiversity* **15**, 346–60.
- Jolivet L and Tamaki K** (1992) Neogene kinematics in the Japan Sea region and volcanic activity of the northeast Japan Arc. *Proceedings of the Ocean Drilling Program, Scientific Results* **127/128**, 1311–31.
- Joye SB, Boetius A, Orcutt BE, Montoya JP, Schulz HN, Erickson MJ and Lugo SK** (2004) The anaerobic oxidation of methane and sulphide reduction in sediments from Gulf of Mexico cold seeps. *Chemical Geology* **205**, 219–38.
- Judd A and Hovland M** (2007) *Seabed Fluid Flow: Impacts on Geology, Biology and Marine Environment*. Cambridge: Cambridge University Press, 475 pp.
- Kaim A, Jenkins RG and Hikida Y** (2009) Gastropods from Late Cretaceous Omagari and Yasukawa hydrocarbon seep deposits in the Nakagawa area, Hokkaido, Japan. *Acta Palaeontologica Polonica* **54**, 463–90.
- Kanehara K** (1937) Miocene shells from the Joban coal-field. *Bulletin of the Imperial Geological Survey of Japan* **27**, 1–12.
- Kanie Y and Kuramochi T** (1995) *Acharax yokosukensis* n.sp. (gigantic bivalve) from Miocene Hayama Formation on the Miura Peninsula, south-central Japan. *Science Reports of Yokosuka City Museum* **43**, 51–7.
- Kanno S** (1955) Tertiary Mollusca from the Taishu Mine, Tsushima, Nagaiki Prefecture, Japan. *Transactions and Proceedings of the Palaeontological Society of Japan* **18**, 31–6.
- Kiel S** (2007) Status of the enigmatic fossil vesicomid bivalve *Pleurophopsis*. *Acta Palaeontologica Polonica* **52**, 639–42.
- Kiel S** (2010) On the potential generality of depth-related ecologic structure in cold-seep communities: evidence from Cenozoic and Mesozoic examples. *Palaeogeography, Palaeoclimatology, Palaeoecology* **295**, 245–57.
- Kiel S** (2013) Lucinid bivalves from ancient methane seeps. *Journal of Molluscan Studies* **79**, 346–63.
- Kiel S, Altamirano AJ, Birgel D, Coxall HK, Hybertsen F and Peckmann J** (2019) Fossiliferous methane-seep deposits from the Cenozoic Talara Basin in northern Peru. *Lethaia* **53**, 166–82.
- Kiel S and Amano K** (2013) The earliest bathymodiolin mussels: an evaluation of Eocene and Oligocene taxa from deep-sea methane-seep deposits in western Washington State, USA. *Journal of Paleontology* **87**, 589–602.
- Kiel S and Hansen B** (2015) Cenozoic methane-seep faunas of the Caribbean region. *PLOS ONE* **10**, e0140788.
- Kiel S, Hybertsen F, Hyžný M and Klompaker AA** (2020) Mollusks and a crustacean from early Oligocene methane-seep deposits in the Talara Basin, northern Peru. *Acta Palaeontologica Polonica* **65**, 109–38.
- Kiel S and Peckmann J** (2007) Chemosymbiotic bivalves and stable carbon isotopes indicate hydrocarbon seepage at four unusual Cenozoic fossil localities. *Lethaia* **40**, 345–57.
- Kiel S and Peckmann J** (2008) Paleocology and evolutionary significance of an Early Cretaceous *Peregrinella*-dominated hydrocarbon-seep deposit on the Crimean Peninsula. *Palaios* **23**, 751–9.
- Kiel S and Taviani M** (2017) Chemosymbiotic bivalves from Miocene methane-seep carbonates in Italy. *Journal of Paleontology* **91**, 444–66.
- Kiel S and Taviani M** (2018) Chemosymbiotic bivalves from late Pliocene Stirone River hydrocarbon seep complex in northern Italy. *Acta Palaeontologica Polonica* **63**, 557–68.
- Kooi H and Groene J** (2001) Offshore continuation of coastal groundwater system; predictions using sharp-interface approximations and variable-density flow modelling. *Journal of Hydrology* **246**, 19–35.
- Krajewski K, Łącka B, Kuźniarski M, Orłowski R and Prejbisz A** (2001) Diagenetic origin of carbonate in Marhøgda Bed (Jurassic) in Spitsbergen, Svalbard. *Polish Polar Research* **22**, 89–128.
- Krajewski K and Luks B** (2003) Origin of “cannon-ball” concretions in the Carolinefjellet Formation (Lower Cretaceous), Spitsbergen. *Polish Polar Research* **24**, 217–42.
- Krajewski K and Woźny E** (2009) Origin of dolomite-ankerite cement in Bravaisberget Formation (Middle Triassic) in Spitsbergen, Svalbard. *Polish Polar Research* **30**, 231–48.
- Krylova EM, Sahling H and Janssen R** (2010) *Abyssogena*: a new genus of the family Vesicomidae (Bivalvia) from deep-water vents and seeps. *Journal of Molluscan Studies* **76**, 107–32.
- Kuechler RR, Birgel D, Kiel S, Freiwald A, Goedert JL, Thiel V and Peckmann J** (2012) Miocene methane-derived carbonates from

- southwestern Washington, USA, and a model of silification at seeps. *Lethaia* **45**, 259–73.
- Kurihara Y** (2007) Occurrence of *Epilucina californica* (Conrad) (Bivalvia: Lucinidae) from the Neogene of Japan, with notes on the biogeographic history of *Epilucina*. *Palaeontological Research* **11**, 29–39.
- Kuroda T** (1931) Fossil mollusca. In *Geology of the Central Part of Shinano* (ed F. Homma), pp. 1–90. Tokyo: Kokin Shoin art. 4 (in Japanese).
- Lallemand S and Jolivet L** (1985) Japan Sea: a pull-apart basin? *Earth and Planetary Science Letters* **76**, 375–89.
- Levin LA and Mendoza GF** (2007) Community structure and nutrition of deep methane-seep macrobenthos from the North Pacific (Aleutian) Margin and the Gulf of Mexico (Florida Escarpment). *Marine Ecology* **28**, 131–51.
- Levin L, Ziebis W, Mendoza G, Growney V, Tryon M, Brown K, Mahn C, Gieskes J and Rathburn A** (2003) Spatial heterogeneity of macrofauna at northern California methane seeps: influence of sulphide concentration and fluid flow. *Marine Ecology Progress Series* **265**, 123–39.
- Little CTS, Birgel D, Boyce AJ, Crame AJ, Francis JE, Kiel S, Peckmann J, Pirrie D, Rollinson GK and Witts JD** (2015) Late Cretaceous (Maastrichtian) shallow water hydrocarbon seeps from Snow Hill and Seymour Islands, James Ross Basin, Antarctica. *Palaeogeography, Palaeoclimatology, Palaeoecology* **418**, 213–28.
- Lorion J, Kiel S, Faure B, Kawato M, Simon YW Ho, Marshall B, Tsuchida S, Miyazaki J-I and Fujiwara Y** (2013) Adaptive radiation of chemosymbiotic deep-sea mussels. *Proceedings of the Royal Society B* **280**, 20131243.
- Machel HG, Mason RA, Mariano AN and Mucci A** (1991) Causes and emission of luminescence in calcite and dolomite. In *Luminescence Microscopy and Spectroscopy: Qualitative and Quantitative Applications* (eds CE Barker and OC Kopp), pp. 9–25, SEPM Short Course no. 25.
- Majima R, Nobuhara T and Kitazaki T** (2005) Review of fossil chemosynthetic assemblages in Japan. *Palaeogeography, Palaeoclimatology, Palaeoecology* **227**, 86–123.
- Masuda K** (1970) Molluscan fauna from the Taishu Group, Tsushima Islands, Nagasaki Prefecture, Japan. *Memoirs of the National Science Museum, Tokyo* **3**, 25–32.
- Mazzini A, Aloisi G, Akhmanov GG, Parnell J, Cronin BT and Murphy P** (2005) Integrated petrographic and geochemical record of hydrocarbon seepage on the Vøring Plateau. *Journal of the Geological Society of London* **162**, 815–27.
- Merz RA** (2015) Textures and traction: how tube-dwelling polychaetes get a leg up. *Invertebrate Biology* **134**, 61–77.
- Miti (The Ministry of International Trade and Industry)** (1972) Report on the regional geological survey, Tsushima, Kamiagata district of the 1971 fiscal year (in Japanese).
- Miti (The Ministry of International Trade and Industry)** (1973) Report on the regional geological survey, Tsushima, Kamiagata district of the 1972 fiscal year (in Japanese).
- Miti (The Ministry of International Trade and Industry)** (1974) Report on the regional geological survey, Tsushima, Kamiagata district of the 1973 fiscal year (in Japanese).
- Miyajima Y, Nobuhara T and Koike H** (2017) Taxonomic reexamination of three vesicomid species (Bivalvia) from the middle Miocene Bessho Formation in Nagano Prefecture, central Japan, with notes on vesicomid diversity. *The Nautilus* **131**, 51–66.
- Miyajima Y, Watanabe Y, Jenkins RG, Goto AS and Hasegawa T** (2018) Diffusive methane seepage in ancient deposits: examples from the Neogene Shin'etsu sedimentary basin, central Japan. *Journal of Sedimentary Research* **88**, 449–66.
- Miyajima Y, Watanabe Y, Yanagisawa Y, Amano K, Hasegawa T and Shimobayashi N** (2016) A Late Miocene methane-seep deposit bearing methane-trapping silica minerals at Joetsu, central Japan. *Palaeogeography, Palaeoclimatology, Palaeoecology* **455**, 1–15.
- Naehr YH, Birgel D, Bohrmann G, MacDonald IR and Kasten S** (2009) Biogeochemical controls on authigenic carbonate formation at the Chapopote “asphalt volcano”, Bay of Campeche. *Chemical Geology* **266**, 390–402.
- Nakada M, Yunagi T and Maeda S** (1997) Lower crustal erosion induced by mantle diapiric upwelling: constraints from the sedimentary basin formation followed by voluminous basalt volcanism in northwest Kyushu, Japan. *Earth and Planetary Science Letters* **146**, 415–29.
- Nakajo T** (1998) Tidal influences on distributary channel sedimentation of the Tertiary delta in the Taishu group, Tsushima Islands, south-west Japan. *Journal of Geosciences, Osaka City University* **41**, 37–46.
- Nakajo T and Funukawa S** (1996) Eocene radiolarians from the Lower Formation of the Taishu Group, Tsushima Islands, Nagasaki Prefecture, Japan. *Journal of the Geological Society of Japan* **102**, 751–4 (in Japanese).
- Nakajo T and Maejima W** (1998) Morpho-dynamic development and facies organization of the Tertiary delta system in the Taishu Group, Tsushima Islands, southwestern Japan. *Journal of the Geological Society of Japan* **104**, 749–63.
- Ninomiya T** (2011) Chemosynthetic fossil molluscan faunas from the Neogene Taishu Group, distributed in Tsushima Island, Nagasaki Prefecture, the south-west Japan. *Memoirs of Faculty of Science, Kyushu University, Series D, Earth and Planetary Science* **32**, 11–26.
- Ninomiya T** (2012) Seep limestone and chemosynthetic fossil assemblages dependent on the seep from the Neogene Taishu Group, Tsushima Island, Nagasaki Prefecture, the southwest Japan. *Science Reports of the Kyushu University, Department of Earth and Planetary Sciences* **23**, 13–21 (in Japanese).
- Ninomiya T, Shimoyama S, Miyata Y, Yamanaka T, Shimazu T, Taniguchi S, Aoki T, Nishida T and Takahashi T** (2020) Origin and water depth of a newly identified seep carbonate and paleoecology of *Bathymodiulus* in the Miocene Taishu Group, southwestern Japan. *Palaeogeography, Palaeoclimatology, Palaeoecology* **546**, 109655.
- Ninomiya T, Shimoyama S, Watanabe K, Horie K, Dunkley D and Shiraishi K** (2014) Age of the Taishu Group, southwestern Japan, and implications for the origin and evolution of the Japan Sea. *Island Arc* **23**, 206–20.
- Ninomiya T, Taniguchi S, Shimoyama S, Watanabe K, Danhara T, Iwano H, Dunkley DJ, Shiraishi K and Gouzu C** (2017) U-Pb and fission-track dating of a submarine pyroclastic rock from southwest Japan. *Island Arc* **26**, e12215.
- Okui A, Kaneko M, Nakanishi S, Monzawa N and Yamamoto H** (2008) An integrated approach to understanding the petroleum system of a frontier deep-water area, offshore Japan. *Petroleum Geoscience* **14**, 223–33.
- Peckmann J, Birgel D and Kiel S** (2009) Microbial fossils reveal fluid composition and flow intensity at a Cretaceous seep. *Geology* **37**, 847–50.
- Peckmann J, Goedert JL, Heinrichs T, Hoefs J and Reitner J** (2003) The late Eocene ‘Whiskey Creek’ methane-seep deposit (western Washington State): petrology, stable isotopes and biogeochemistry. *Facies* **48**, 241–54.
- Peckmann J, Goedert JL, Thiel V, Michaelis W and Reitner J** (2002) A comprehensive approach to the study of methane-seep deposits from the Lincoln Creek Formation, western Washington State, USA. *Sedimentology* **49**, 855–73.
- Peckmann J, Kiel S, Sandy MR, Taylor DG and Goedert JL** (2011) Mass occurrences of the brachiopod *Halorella* in Late Triassic methane-seep deposits, eastern Oregon. *Journal of Geology* **119**, 207–20.
- Peckmann J, Sandy MR, Taylor DG, Gier S and Back W** (2013) An Early Jurassic brachiopod-dominated seep deposit enclosed by serpentinite, eastern Oregon, USA. *Palaeogeography, Palaeoclimatology, Palaeoecology* **390**, 4–16.
- Peckmann J, Senowbari-Daryan B, Birgel D and Goedert JL** (2007) The crustacean ichnofossil *Palaxius* associated with callianassid body fossils in an Eocene methane-seep limestone, Humptulips Formation, Olympic Peninsula, Washington. *Lethaia* **40**, 273–80.
- Peckmann J and Thiel V** (2004) Carbon cycling at ancient methane seeps. *Chemical Geology* **205**, 443–67.
- Peckmann J, Walliser OH, Riegel W and Reitner J** (1999) Signatures of hydrocarbon venting in a Middle Devonian carbonate mound (Holland Mound) at the Hamar Laghdad (AntiAtlas, Morocco). *Facies* **40**, 281–96.
- Peters KE, Walters CC and Moldovan MJ** (2005) *The Biomarker Guide. Volume 1: Biomarkers and Isotopes in the Environment and Human History*. Cambridge: Cambridge University Press, 471 pp.

- Pye K, Dickson JAD, Schiavon N, Coleman ML and Cox M** (1990) Formation of siderite–Mg–calcite–iron sulphide concretions in intertidal marsh and sandflat sediments, north Norfolk, England. *Sedimentology* **37**, 325–43.
- Reinter J, Peckmann J, Blumenberg M, Michaelis W, Reimer A and Thiel V** (2005) Concretionary methane-seep carbonates and associated microbial communities in Black Sea sediments. *Palaeogeography, Palaeoclimatology, Palaeoecology* **227**, 18–30.
- Rio M, Roux M, Renard M and Schein E** (1992) Chemical and isotopic features of present day bivalve shells from hydrothermal vents and cold seeps. *Palaios* **7**, 351–60.
- Ritt B, Sarazzin J, Caprais J-C, Noël P, Gauthier O, Pierre C, Henry P and Desbruyères D** (2010) First insights into the structure and environmental setting of cold-seep communities in the Marmara Sea. *Deep-Sea Research Part I: Oceanographic Research Papers* **57**, 1120–36.
- Saether KP, Little CTS and Campbell KA** (2010a) A new fossil provannid gastropod from Miocene hydrocarbon seep deposit, East Coast Basin, New Zealand. *Acta Palaeontologica Polonica* **55**, 507–17.
- Saether KP, Little CTS, Campbell KA, Marshall BA, Collins M and Alfaro AC** (2010b) New fossil mussels (Bivalvia: Mytilidae) from Miocene hydrocarbon seep deposits, North Island, New Zealand, with general remarks on vent and seep mussels. *Zootaxa* **2577**, 1–45.
- Sakai H and Nishi H** (1990) Geological ages of the Taishu Group and the Katsumoto Formation in the Tsushima and Iki Islands, off the northwest Kyushu on the basis of planktonic foraminifers. *Journal of the Geological Society of Japan* **96**, 389–92.
- Savard MM, Beachamp B and Veizer J** (1996) Significance of aragonite cements around Cretaceous marine methane seeps. *Journal of Sedimentary Research* **66**, 430–8.
- Senowbari-Daryan B, Gaillard C and Peckmann J** (2007) Crustacean microprolites from Jurassic (Oxfordian) hydrocarbon seep deposits of Beauvoisin, southeastern France. *Facies* **53**, 229–38.
- Sibuet M and Olu K** (1998) Biogeography, biodiversity and fluid dependence of deep-sea cold-seep communities at active and passive margins. *Deep-Sea Research II* **45**, 517–67.
- Smith GL, McNiell LC, Henstock TJ, Arraiz D and Spiess V** (2014) Fluid generation and distribution in the highest sediment input accretionary margin, the Makran. *Earth and Planetary Science Letters* **403**, 131–43.
- Smrzka D, Kraemer SM, Zwicker J, Birgel D, Fischer D, Kasten S, Goedert JL and Peckmann J** (2015) Constraining silica diagenesis in methane-seep deposits. *Palaeogeography, Palaeoclimatology, Palaeoecology* **420**, 13–26.
- Smrzka D, Zwicker J, Misch D, Walkner C, Gier S, Monien P, Bohrmann G and Peckmann J** (2019) Oil seepage and carbonate formation: a case study from the southern Gulf of Mexico. *Sedimentology* **66**, 2318–53.
- Squires R** (1995) First fossil species of the chemosynthetic-community gastropod *Provanna*: localized cold-seep limestones in upper Eocene and Oligocene rocks, Washington. *The Veliger* **38**, 30–6.
- Tanaka K** (1959) Molluscan fossils from central Shinano, Nagano Prefecture, Japan (Part 1) – fossils from Akanuda limestone. *Journal of Shinshu University, Faculty of Education* **8**, 115–33.
- Tsuchi R** (1990) Neogene events in Japan and the Pacific. *Palaeogeography, Palaeoclimatology, Palaeoecology* **77**, 355–65.
- Turnipseed M, Jenkins CD and Van Dover CL** (2004) Community structure in Florida Escarpment seep and Snake Pit (Mid-Atlantic Ridge) vent mussel beds. *Marine Biology* **145**, 121–32.
- Van Winkle K** (1919) Remarks on some new species from Trinidad. *Bulletins of American Paleontology* **8**, 19–27.
- Walliser EO, Tanabe K, Hilkida Y, Shirai K and Schöne BR** (2019) Sclerochronological study of the gigantic inoceramids *Sphenoceramus schmidti* and *S. sachalinensis* from Hokkaido, northern Japan. *Lethaia* **52**, 410–28.
- Wefer G, Berger WH, Richter C and Shipboard Scientific Party** (1998) Facies patterns and authigenic minerals of upwelling deposits off Southwest Africa. *Proceedings of the Ocean Drilling Program* **175**, 487–504.
- Whiticar MJ** (1999) Carbon and hydrogen isotope systematics of bacterial formation and oxydation of methane. *Chemical Geology* **161**, 291–314.
- Xu T, Feng D, Tao J and Qui W-J** (2019) A new species of deep-sea mussel (Bivalvia: Mytilidae: *Gigantidas*) from the South China Sea: morphology, phylogenetic position, and gill-associated microbes. *Deep-Sea Research I: Oceanographic Research Papers* **146**, 79–90.
- Zitter TAC, Henry P, Aloisi G, Delaygue G, Çagatay MN, Mercier de Lepinay B, Al-Samir B, Fornacciari F, Tesmer TM, Pekdeger A, Wallmann K and Lericolais G** (2008) Cold seeps along the main Marmara Fault in the Sea of Marmara (Turkey). *Deep-Sea Research Part I: Oceanographic Research Papers* **55**, 552–70.
- Zwicker J, Smrzka D, Gier S, Goedert JL and Peckmann J** (2015) Mineralized conduits are parts of the uppermost plumbing system of Oligocene methane-seep deposits, Washington State (USA). *Marine and Petroleum Geology* **66**, 616–30.
- Zwicker J, Smrzka D, Himmler T, Monien P, Gier S, Goedert JL and Peckmann J** (2018) Rare earth elements as tracers for microbial activity and early diagenesis: a new perspective from carbonate cements of ancient methane-seep deposits. *Chemical Geology* **501**, 77–85.